Ocean Modelling 43–44 (2012) 112–137

Contents lists available at SciVerse ScienceDirect

Ocean Modelling

journal homepage: www.elsevier.com/locate/ocemod

Ocean–atmosphere dynamics during Hurricane Ida and Nor'Ida: An application of the coupled ocean–atmosphere–wave–sediment transport (COAWST) modeling system

Maitane Olabarrieta [a,*], John C. Warner [a], Brandy Armstrong [a], Joseph B. Zambon [b], Ruoying He [b]

[a] US Geological Survey, Woods Hole Coastal and Marine Science Center, 384 Woods Hole Road, Woods Hole, MA 02543, United States
[b] Department of Marine, Earth and Atmospheric Sciences, North Carolina State University, Raleigh, NC 27695, United States

ARTICLE INFO

Article history:
Received 22 March 2011
Received in revised form 18 December 2011
Accepted 19 December 2011
Available online 30 December 2011

Keywords:
COAWST model
Hurricane
Tropical storm
Extra tropical storm
Runup
Storm surge
Nor'Ida
Coupled model
Air–sea interaction
Wave age
Wave steepness
Ocean wave roughness
SWAN
ROMS
WRF

ABSTRACT

The coupled ocean–atmosphere–wave–sediment transport (COAWST) modeling system was used to investigate atmosphere–ocean–wave interactions in November 2009 during Hurricane Ida and its subsequent evolution to Nor'Ida, which was one of the most costly storm systems of the past two decades. One interesting aspect of this event is that it included two unique atmospheric extreme conditions, a hurricane and a nor'easter storm, which developed in regions with different oceanographic characteristics. Our modeled results were compared with several data sources, including GOES satellite infrared data, JASON-1 and JASON-2 altimeter data, CODAR measurements, and wave and tidal information from the National Data Buoy Center (NDBC) and the National Tidal Database. By performing a series of numerical runs, we were able to isolate the effect of the interaction terms between the atmosphere (modeled with Weather Research and Forecasting, the WRF model), the ocean (modeled with Regional Ocean Modeling System (ROMS)), and the wave propagation and generation model (modeled with Simulating Waves Nearshore (SWAN)). Special attention was given to the role of the ocean surface roughness. Three different ocean roughness closure models were analyzed: DGHQ (which is based on wave age), TY2001 (which is based on wave steepness), and OOST (which considers both the effects of wave age and steepness). Including the ocean roughness in the atmospheric module improved the wind intensity estimation and therefore also the wind waves, surface currents, and storm surge amplitude. For example, during the passage of Hurricane Ida through the Gulf of Mexico, the wind speeds were reduced due to wave-induced ocean roughness, resulting in better agreement with the measured winds. During Nor'Ida, including the wave-induced surface roughness changed the form and dimension of the main low pressure cell, affecting the intensity and direction of the winds. The combined wave age- and wave steepness-based parameterization (OOST) provided the best results for wind and wave growth prediction. However, the best agreement between the measured (CODAR) and computed surface currents and storm surge values was obtained with the wave steepness-based roughness parameterization (TY2001), although the differences obtained with respect to DGHQ were not significant. The influence of sea surface temperature (SST) fields on the atmospheric boundary layer dynamics was examined; in particular, we evaluated how the SST affects wind wave generation, surface currents and storm surges. The integrated hydrograph and integrated wave height, parameters that are highly correlated with the storm damage potential, were found to be highly sensitive to the ocean surface roughness parameterization.

Published by Elsevier Ltd.

1. Introduction

Extreme storms such as hurricanes and extratropical storms can play a significant role in shaping the beaches of the East and Gulf Coasts of the United States (Dolan and Hayden, 1981; Dolan and Davis, 1994; Lee et al., 1998). The Assessment Report from the Intergovernmental Panel of Climate Change (the IPCC, 2007) states that future tropical depressions will become more numerous and more likely to develop into major hurricanes than in the present climate, and thus they will have greater potential to impact the coast. Multiple studies have attempted to define the relationship between coastal damage and storm parameters such as duration, wind speed, and total water level. Irish and Resio (2010) presented a hydrodynamics-based surge scale for hurricanes. Sallenger (2000) proposed four different storm impact regimes defined by coastal morphology and total water levels. More recently, Munger and Kraus (2010) computed the beach erosion on Northern

* Corresponding author. Tel.: +1 508 5245009.
E-mail address: molabarrieta@usgs.gov (M. Olabarrieta).

1463-5003/$ - see front matter Published by Elsevier Ltd.
doi:10.1016/j.ocemod.2011.12.008

Assategue Island under different historical storm conditions. They observed that in the case of tropical storms such as hurricanes, the erosion is strongly correlated with the integrated wave height and, to a lesser extent, with the storm duration and integrated hydrograph. For extratropical storms, the opposite was found, with erosion more significantly correlated with the integrated hydrograph and, to a lesser extent, with the integrated wave height and storm duration. Similar conclusions were reached by Herrington and Miller (2010) who used different methods to calculate the damage potential of nor'easter storms.

Numerical models provide a useful approach to study the spatial and temporal distribution of parameters, including the significant wave height, the storm surge, the integrated hydrograph, and the integrated wave height, during all types of storm events. Simulation of historical events and correlation analysis of the predictions with the observed coastal damage and erosion can lead to the derivation of more precise storm impact indexes. Numerical models can also be used to forecast incoming storms, and they can therefore provide the basis for coastal erosion and damage warning systems.

The correct estimation of the impact of a storm, including the total water levels and the wind wave heights, using numerical modeling requires an accurate representation of the air–sea interaction dynamics, a highly complex relationship due to the variable interactions between wind, ocean waves and currents near the sea surface. For example, Chen et al. (2007) remarked that coupling the atmospheric models with an ocean circulation model that includes a realistic thermal stratification and vertical mixing is necessary to ensure the adequate representation of hurricane intensity. Other studies (Döscher et al., 2002; Aldrian et al., 2005; Loglisci et al., 2004) have demonstrated that atmosphere and ocean coupling is also necessary for the correct simulation of other meteorological extreme conditions. Because storm surge and wind waves are highly sensitive to wind direction and intensity, it is critical to correctly simulate the atmospheric dynamics and the air–sea momentum transfer processes. Kim et al. (2010) pointed out that wave-current interactions could also be relevant to the storm surge evaluation.

To better understand the mechanisms of the air–sea interaction, different coupled numerical models that consider atmosphere and ocean interaction have been developed in recent decades (Gustafsson et al., 1998; Hagedorn et al., 2000; Schrum et al. 2003; Döscher et al., 2002; Ren et al., 2004; Aldrian et al., 2005; Mikolajewicz et al., 2005; Seo et al., 2007; Bender and Ginis, 2000; Bender et al., 2007; Yao et al., 2008). The application of these models to actual storm events has shown that the flux coupling between the ocean and the atmosphere improves the simulation of the air dynamics over an atmospheric model using a prescribed SST. A more complete summary of atmosphere–ocean coupled models is provided by Seo et al. (2007). Perrie et al. (2004, 2005) included the effect of the sea spray on an atmosphere–ocean coupled model and observed that sea spray enhances sea surface heat fluxes and slightly increases the maximum intensity of extratropical Hurricane Gustav (2002).

The analysis of surge levels under storm conditions is usually accomplished with coupled ocean-wave models (Kim et al., 2010). Mastenbroek et al. (1993) and Zhang and Li (1997) coupled a surge and a wave model through 2D radiation stresses and surge-induced currents, without considering the nearshore wind wave transformation. Xie et al. (2008) applied the POM-SWAN coupled model for inundation predictions in Charleston Harbor during Hurricane Hugo in 1989, showing that radiation stresses caused significant changes to inundation. Funakoshi et al. (2008), Chen et al. (2008), and Kim et al. (2010) used coupled ocean-wave models to analyze water levels during Hurricane Floyd (1999), Hurricane Katrina (2005), and Typhoon Anita (1970), respectively. Sheng et al. (2010) investigated the effects of waves on storm surges, currents, and inundation in the region of the Outer Banks and Chesapeake Bay during Hurricane Isabel 2003). Their analysis revealed noticeable effects of waves on the storm surge, currents and inundation. They concluded that the radiation stress terms and wave-induced stresses have a greater effect than wave-induced bottom stresses on water levels. Fan et al. (2009b) analyzed the performance of WaveWatchIII during a strong tropical cyclone (Hurricane Ivan, 2004) using various drag coefficient parameterizations for the wind shear stress and ocean current inputs. It is noteworthy that in these coupled wave–ocean models, the wind forcing and the atmospheric pressure (if considered) are derived from the results of atmospheric models that do not include dynamic feedback from the ocean. However, when computing the wind shear stress, the effect of the wave-induced stress (Donelan et al., 1993; Janssen, 1989; Hara and Belcher, 2002) is taken into account.

It was not until the last decade that atmosphere–wave–ocean models were developed. Powers and Stoelinga (2000) presented a comprehensive atmosphere–ocean–wave modeling system and performed sensitivity tests on the surface roughness parameterization of the atmospheric model MM5. They showed that a roughness parameterization that takes into account the wave age can significantly improve the calculation of surface wind stress and heat flux. Chen et al. (2007) described the development of a fully coupled atmosphere–wave–ocean model for hurricane research and prediction. This model includes the wind-wave parameterization developed by the CBLAST-Hurricane modeling team that incorporates the effects of the wave spectral tail of the wind drag coefficient. The application of this model to Hurricane Frances (2004) showed that the coupled model, with the new drag parameterization, improved the accuracy of the modeled storm structure and intensity. Although this model includes advanced air–ocean–wave interaction closure models, it does not include the effects of the waves on the ocean model and does not consider the wave-induced currents and the turbulence generation due to wave dissipation, which is potentially relevant for storm surge prediction.

The goal of the present study is to increase our understanding of atmosphere–ocean–wave interactions and their role in storm surge and wind wave prediction using the COAWST modeling system (Warner et al., 2010). COAWST incorporates air–sea and wave-hydrodynamics interactions, and during a previous study of Hurricane Isabel (2003), it was used to demonstrate that (1) hurricane intensity is extremely sensitive to SST, ocean currents, and waves and that (2) wave characteristics are sensitive to both ocean and atmospheric coupling. In the current study, COAWST is used to model Hurricane Ida and its evolution into Nor'Ida, a storm event that impacted the US East Coast in November 2009. We investigated the effects of various modeled interactions by conducting multiple numerical simulations in which different interaction processes were considered or neglected. Comparison of the simulated winds, waves, currents, and sea elevations with observations revealed the relative importance of the various interaction terms for capturing storm dynamics along the US East Coast. Furthermore, we studied the sensitivity of the integrated significant wave height and integrated hydrograph to these interaction terms.

2. Methodology

The coupled ocean–atmosphere–wave–sediment transport (COAWST) modeling system (Warner et al., 2010) was used in this study. This modeling system couples 3 components, which are described below: a non-hydrostatic meteorological model (WRF), a three-dimensional hydrostatic ocean model (ROMS) and a wave generation and propagation model (SWAN). Model Coupling

Toolkit (MCT) was used to enable the interaction between these components. Observational data, described below, were used for model analysis.

2.1. Atmospheric module

The atmospheric model component in the coupled system is the Weather Research and Forecasting (WRF) model (Skamarock et al., 2005). This model has been used extensively for operational forecasts, as well as for realistic and idealized research experiments. The WRF distribution includes a choice of 2 dynamical solvers, the Non-hydrostatic Mesoscale Modeler (NMM) and the Advanced Research WRF (ARW) cores. This study utilizes the ARW core, which is configured as a non-hydrostatic, fully compressible atmospheric model with physics schemes and a variety of physical parameterizations of sub-grid scale processes for predicting meso- and microscale motion. The model predicts three-dimensional wind momentum components, surface pressure, dew point, precipitation, surface-sensible and latent heat fluxes, relative humidity, and air temperature on a sigma-pressure vertical coordinate grid.

In the present study, WRF is run on a 6 km horizontal resolution numerical grid, covering the region shown in Fig. 1(a), with 28 sigma levels. A 2 km vortex following a nested grid was initialized in the Yucatan Strait to provide higher resolution for the modeling of Hurricane Ida. In both grids, we used the Kain–Fritsch (K-F) cumulus parameterization (Kain and Fritsch, 1993) and an explicit, 5-class (cloud, rain, ice, snow, graupel) microphysics scheme based on Lin et al. (1983). The planetary boundary layer was modeled with the Mellor–Yamada Nakanishi Niino (MYNN) level 2.5 (Nakanishi, 2001; Nakanishi and Niino 2004, 2006, 2009) closure scheme. The WRF module is coupled to the ocean module by including the effect of the high temporal and spatial resolution SST computed in ROMS, which affects the flux transfer in the atmospheric boundary layer. If this coupling is not activated, WRF considers the lower resolution (0.5 degrees) daily Real-Time Global (RTG) Sea Surface Temperature SST field provided by NCEP (Gemmill et al., 2007; ftp://polar.ncep.noaa.gov/pub/history/sst). When WRF is not coupled to a wave model, the bottom roughness is computed with the formulation proposed by Smith (1988), which is a combination of the formulas described by Liu et al. (1979) and Charnock (1955, hereinafter CHNK). When WRF is coupled to a wave model, there are three methods for including enhanced bottom roughness at the sea surface. Warner et al. (2010) included an enhanced bottom roughness (KWS) based on the formulation of Taylor and Yelland (2001; hereinafter TY2001) when computing the bottom stress over the ocean. This closure model, as shown by Drennan et al. (2005), provides a good estimation of the ocean roughness under swell conditions, whereas in young sea states, it underestimates the sea roughness. For this study, two more formulations were implemented. A second method, that of Drennan et al. (2003; hereinafter DGHQ) proposed another closure model based on wave age scaling (but neglecting wave steepness), showing a better performance for young sea states. The third method, Oost et al. (2002; hereinafter OOST) proposed a different relationship that is also dependent on the wave age but which indirectly takes into account the effect of the wave steepness. To analyze the effect induced by considering different closure models for the sea surface roughness, all the aforementioned formulations were implemented in the WRF model. A more detail description of these closure models is presented in Appendix A.

The hindcast simulations were initialized on the 8th of November 2009 at 12:00 UTC (Coordinated Universal Time) using data from the National Centers for Environmental Prediction (NCEP) Global Forecast Model (GFS), obtained on a 1 degree grid. The same database, with a 6 h time resolution, was used to derive the boundary conditions. Because the resolution of the initial condition derived from the GFS data was not sufficiently high to correctly simulate the hurricane, the initial conditions derived from the GFS model were modified following the method used by Warner et al. (2010), assigning the initial hurricane strength and intensity to the observed values. The atmospheric model required 1 day for the spinup (shown in the results section), and therefore, the results corresponding to that day were not considered in the verification section. Modification of the initial condition, as well as the implementation of the vortex, following application of the high-resolution grid was necessary for the correct simulation of the hurricane system.

2.2. Hydrodynamic module

The Regional Ocean Modeling System (ROMS) is a three-dimensional, free surface, terrain following numerical model that solves

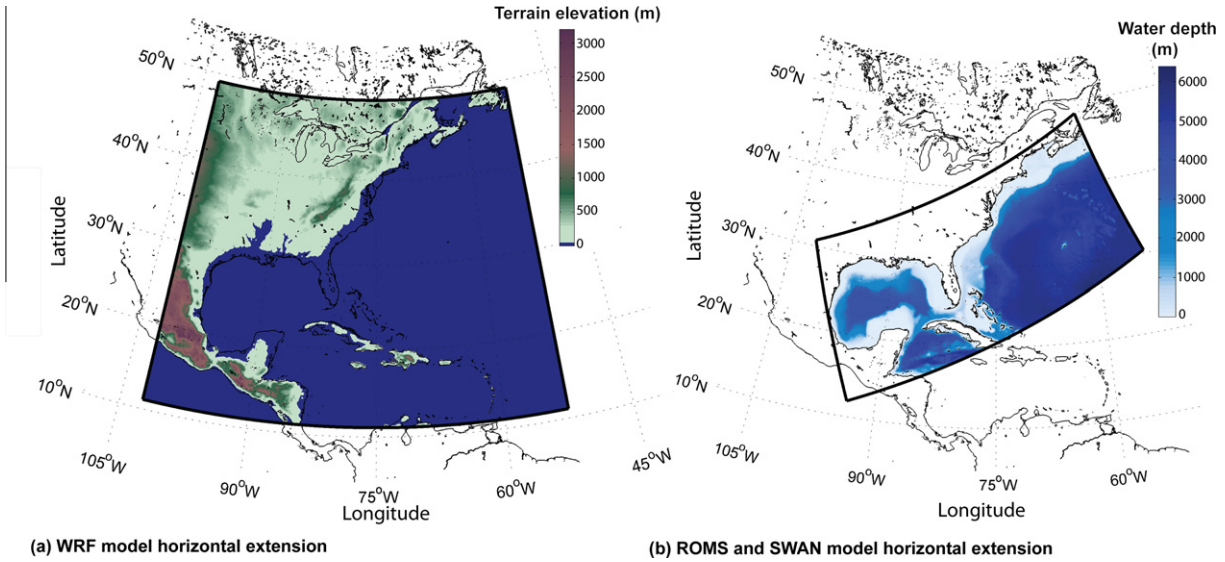

Fig. 1. (a) Horizontal extension and the terrain elevation of the numerical grid used in WRF. (b) Horizontal extension and bathymetry of the numerical grid used in ROMS and SWAN.

finite-difference approximations of the Reynolds–Averaged Navier–Stokes (RANS) equations using the hydrostatic and Boussinesq assumptions (Chassignet et al., 2000; Haidvogel et al., 2000) with a split-explicit time stepping algorithm (Shchepetkin and McWilliams, 2005; Haidvogel et al., 2008).

In ROMS, the effects of surface waves are included using three different mechanisms:

(1) The enhancement of the apparent bed roughness due to the effect of turbulence in the wave boundary layer (KAW), which is parameterized using the formulation proposed by Madsen (1994).
(2) The turbulent kinetic energy injection during wave breaking (TKE), introduced as a surface flux of turbulence kinetic energy in the GLS method (Warner et al., 2005). In the present study, the surface flux is considered to be proportional to the net energy dissipated during the breaking process (Feddersen and Trowbridge, 2005) and the surface roughness is proportional to the significant wave height (Stacey, 1999).
(3) In the present application, the wave forces are included using the VF formalism following the methodology presented by Uchiyama et al. (2010) and included in the COAWST system by Kumar et al. (2012).

The effect of these formulations on ocean–atmosphere–wave interactions will be presented in a different study.

The interaction of ocean and atmospheric models occurs with momentum and heat fluxes. Recent developments of the COAWST system include the transference of the momentum and heat fluxes from WRF to ROMS using a flux-conservative remapping scheme, which differs from the bulk approximations made in Warner et al. (2010). In this way, both modules (WRF and ROMS) use the same quantities of fluxes at the ocean–atmosphere interface. The momentum and heat fluxes are computed using the TY2001; DGHQ or OOST closure models, as previously described. If the effect of the waves is not taken into account in the momentum exchange between the ocean and the atmosphere, the CHNK closure model is considered for the surface roughness.

In this application, ROMS used a 5 km horizontal resolution grid with 16 vertically stretched θ layers (Fig. 1(b)). The vertical stretching parameters were $\theta_s = 10$, $\theta_b = 0.4$ and $T_{\text{cline}} = 50$ m. These were the stretching values that resulted in the best agreement between the CODAR data and the currents affecting the wave field. The hydrodynamic model was spunup from the 1st of October until the 8th of November at 12 UTC (without being coupled to WRF and SWAN), with North American Regional Reanalysis (NARR) atmospheric forcing. It was initialized using the outputs of HYCOM GLBa0.08 from the Naval Research Laboratory. The model was nudged to the HYCOM GLBa0.08 model's temperature, with a 1 day nudging coefficient. The WRF–ROMS–SWAN coupled model was initialized on the 8th of November 2009 at 12:00 UTC with the initial condition derived from the spinup. In both the spinup and the fully coupled runs, the same database (HYCOM GLBa0.08 with a 1 day temporal resolution and 1/12 degrees spatial resolution) was used to derive the lateral boundary conditions. At the boundaries, a nudging boundary condition was imposed for the temperature and salinity fields as well as for the baroclinic velocities. A Flather boundary condition (Flather, 1976) for the barotropic currents was imposed in the open boundaries, allowing for the free propagation of wind-generated currents and tides. River inputs were not directly considered in the present study.

2.3. Wind wave module

Simulating WAves in the Nearshore (SWAN; Booij et al., 1999), a phase-averaged wave model, is used in the COAWST system. This model solves the transport equations for wave action density and accounts for shoaling and refraction, wind-wave generation, wave breaking, bottom dissipation, and nonlinear wave-wave interactions. SWAN can be run concurrently with the ocean and the atmosphere models, allowing currents and sea surface elevations to influence the wave field and waves to affect the circulation and atmosphere dynamics.

In the present application, SWAN was run in the same grid as ROMS (Fig. 1(b)) and was forced with the wind fields computed by WRF. Twenty-five frequency (0.01–1 Hz) and sixty directional bands were used. The boundary conditions were derived from the WaveWatchIII model, which is operationally run at NOAA.

In the coupled system, the free surface elevations and currents are provided to SWAN by ROMS. The currents were computed according to the formulation presented by Kirby and Chen (1989), in which the vertical distribution of the current profile is taken into account, as well as the relative water depth of the surface waves. WRF provides SWAN with the surface winds used in the Komen et al. (1984) closure model for the exponential energy transfer from the atmosphere to the wind wave field.

As shown in Fig. 1, two different grids have been used to run the COAWST system. The Model Coupling Toolkit (MCT; Larson et al., 2004; Jacob et al., 2005) and the Spherical Coordinate Remapping Interpolation Package (SCRIP; Jones, 1998) allow the transmission of regridded data between the model components. For a more complete description of the coupled system, the reader is referred to Warner et al. (2008, 2010). In this specific model setting, the baroclinic time step used in ROMS was 120 s with a time splitting ratio of 30. SWAN ran with a 300 s time step, and WRF ran with a 25 s time step. The data interchange between the models occurred every 1200 s.

2.4. Observational data sources

2.4.1. Wave buoys and tide gauges

In this study, we used wind and wave measurements from 50 NDBC (National Data Buoy Center) wave buoys distributed along the US East Coast (Fig. 2(a)). The relative error for the significant wave height (H_s) as measured by these buoys is generally predicted to be a few percent. In the high wave range, the buoys have a tendency to slip around the highest crests, introducing a negative bias in the estimate of the higher values. The sea surface elevations from 60 tidal gauges of the NOAA Tidal Gauge database were used to obtain the storm surge value (Fig. 2(b)).

2.4.2. CODAR data

Based on a 22-station HF Radar Network, the Mid-Atlantic Regional Coastal Ocean Observing System (MARCOOS) collects surface current data between Cape Cod and Cape Hatteras. The HF Radar uses the Doppler Shift of a radio signal that is backscattered off the ocean surface to measure the flow component in the antenna direction. The CODAR radial spectra's resolution is dependent on the operating frequency, the sweep rate, and the FFT length used in processing. The CODAR data were processed considering a standard 1 Hz sweep rate, an operating frequency of 4.55 MHz, and a 1024-point FFT, which gives a radial velocity resolution of 3.22 cm s^{-1} (Gong et al., 2010). The final total vector current map has a spatial resolution of 6 km with a cross-shelf range of 150 km. The averaged current fields were constructed using the 3 hourly total vector maps.

2.4.3. Satellite data

Three different satellite data sets were used: JASON-1 and JASON-2 altimeter data and GOES infrared data. The JASON-1 and JASON-2 altimeters are used to compute wind speed and significant wave height measurements. These satellites follow an orbit with a

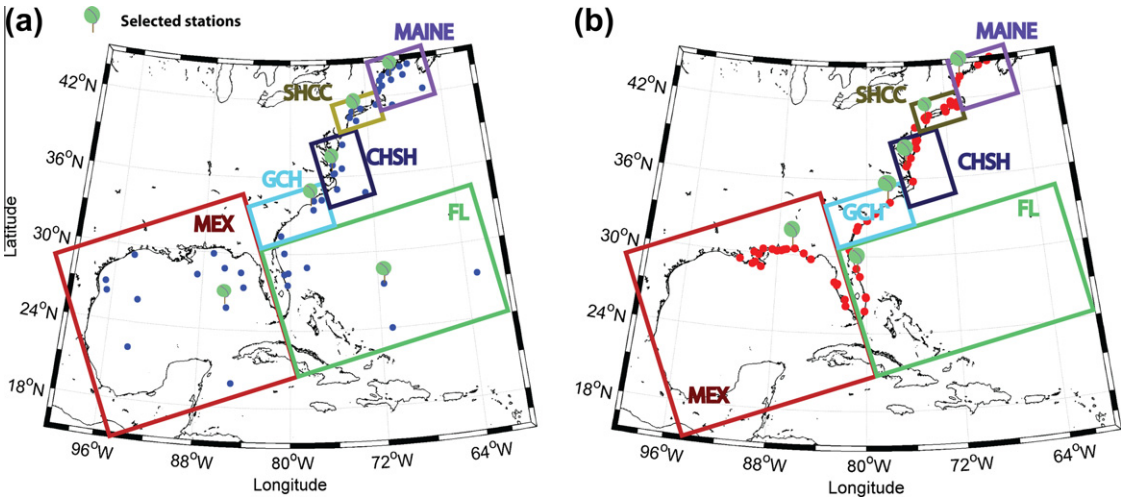

Fig. 2. (a) Location of the considered NDBC wave buoys. (b) Location of the considered tidal gauges from the NOAA Tidal Gauge database.

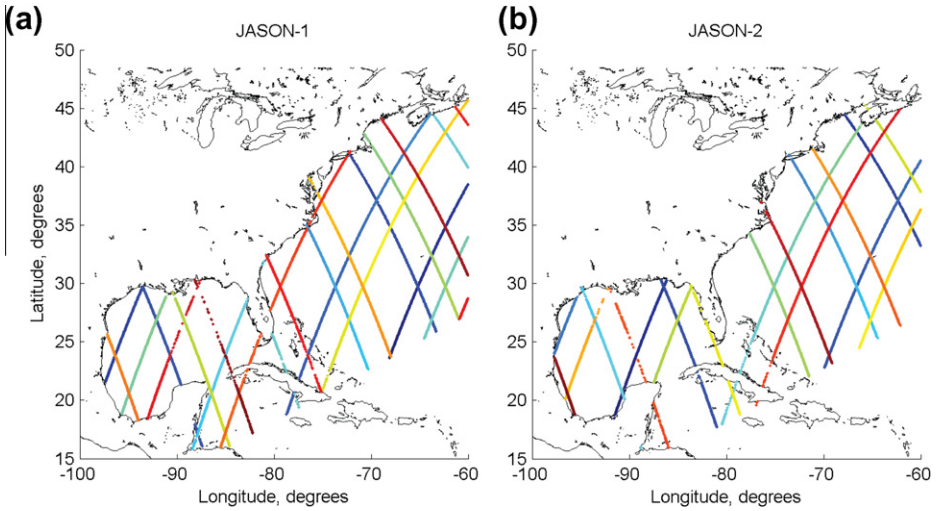

Fig. 3. Ground track of the (a) JASON-1 and (b) JASON-2 satellites for the analysis period and the study region.

10 day period and have an along-track resolution of 5.8 km (Fig. 3). To identify the position and time of each sample, the colors in Fig. 3 correspond to the sample number. The first measurements (corresponding to the 9th of November) are presented in deep blue, and the last measurements (corresponding to the 16th of November) are presented in deep red. Only measurements from the *Ku-band* were used in this study as they are known to have higher accuracy than the *C-band*. Based on the altimeter data, the wind speed is computed through the Gourrion algorithm (Gourrion et al., 2002), a neural network that relates the *Ku-band* backscatter coefficient to significant wave height. This purely empirical wind speed function takes into account the sea-state effect on the altimeter-derived backscatter. It is used to evaluate the wind speed 10 meters above the sea surface and is considered to be accurate to 2 m s^{-1} (OSTM/JASON-2 Products Handbook). Cavaleri and Sclavo (2006) described some of the limitations of these data sets. For example, the wind speeds from the altimeters are only reliable at magnitudes between 2 m s^{-1} and 20 m s^{-1}. Additionally, altimeter-measured significant wave heights become unreliable at large values (>20 m).

The SST data were obtained from the NOAA CoastWatch, which provides sea surface temperature products derived from NOAA's Geostationary Operational Environmental Satellites (GOES). The GOES data used for the analysis have a 4 km spatial and a 3 h temporal resolution. GOES SST is determined by applying an algorithm to the level infrared data. Multispectral information is used to identify clouds, wind effects, and other factors that may affect the values. The validation of these algorithms showed that the GOES-Buoy SST has a bias of 0.5 °C with a standard deviation of less than 1 °C.

2.4.4. Surface wind analysis data

Marine wind gridded data from the Wind Analysis products created by NOAA's Hurricane Research Division (http://www.aoml.noaa.gov/hrd/Storm_pages/ida2009/wind.html) were used in the present study. These wind fields are derived by applying objective analysis methods (Powell et al., 1996; Powell and Houston, 1996) to data that are collected by the Air Force and by NOAA aircrafts, ships, buoys, coastal platforms, surface aviation reports, and reconnaissance aircraft and then adjusted to the surface.

3. Model application

Hurricane Ida, which originated off the eastern coast of Nicaragua on the 4th of November, was the strongest landfalling tropical

Table 1
Ocean–atmosphere–wave coupling interactions considered in the numerical runs.

	SWAN EFFECTS CONSIDERED IN WRF	ROMS EFFECTS CONSIDERED IN WRF	WRF EFFECTS CONSIDERED IN SWAN				ROMS EFFECTS CONSIDERED IN SWAN		WRF EFFECTS CONSIDERED IN ROMS				SWAN EFFECTS CONSIDERED IN ROMS			
Run	KWS	SST	WINDS COMPUTED WITH DIFFERENT OCEAN ROUGHNESS CLOSURE MODELS FOR WRF BBL				ELV	CUR	WIND SHEAR STRESS AND HEAT AND MOISTURE FLUXES COMPUTED WITH DIFFERENT OCEAN ROUGHNESS CLOSURE MODELS FOR WRF BBL				VF	KAW	TKE	COMMENTS
			CHNK	DGHQ	TY2001	OOST			CHNK	DGHQ	TY2001	OOST				
R1	×	×	✓	×	×	×	✓	✓	✓	×	×	×	✓	✓	✓	CHNK ocean roughness and no high resolution SST to WRF
R2	×	✓	✓	×	×	×	✓	✓	✓	×	×	×	✓	✓	✓	Coupled, but with CHNK wave induced ocean roughness
R3	✓	✓	×	✓	×	×	✓	✓	×	✓	×	×	✓	✓	✓	Fully coupled baseline, with DGHQ ocean roughness
R4	✓	✓	×	×	✓	×	✓	✓	×	×	✓	×	✓	✓	✓	Fully coupled baseline, with TY2001 ocean roughness
R5	✓	✓	×	×	×	✓	✓	✓	×	×	×	✓	✓	✓	✓	Fully coupled baseline, with OOST ocean roughness

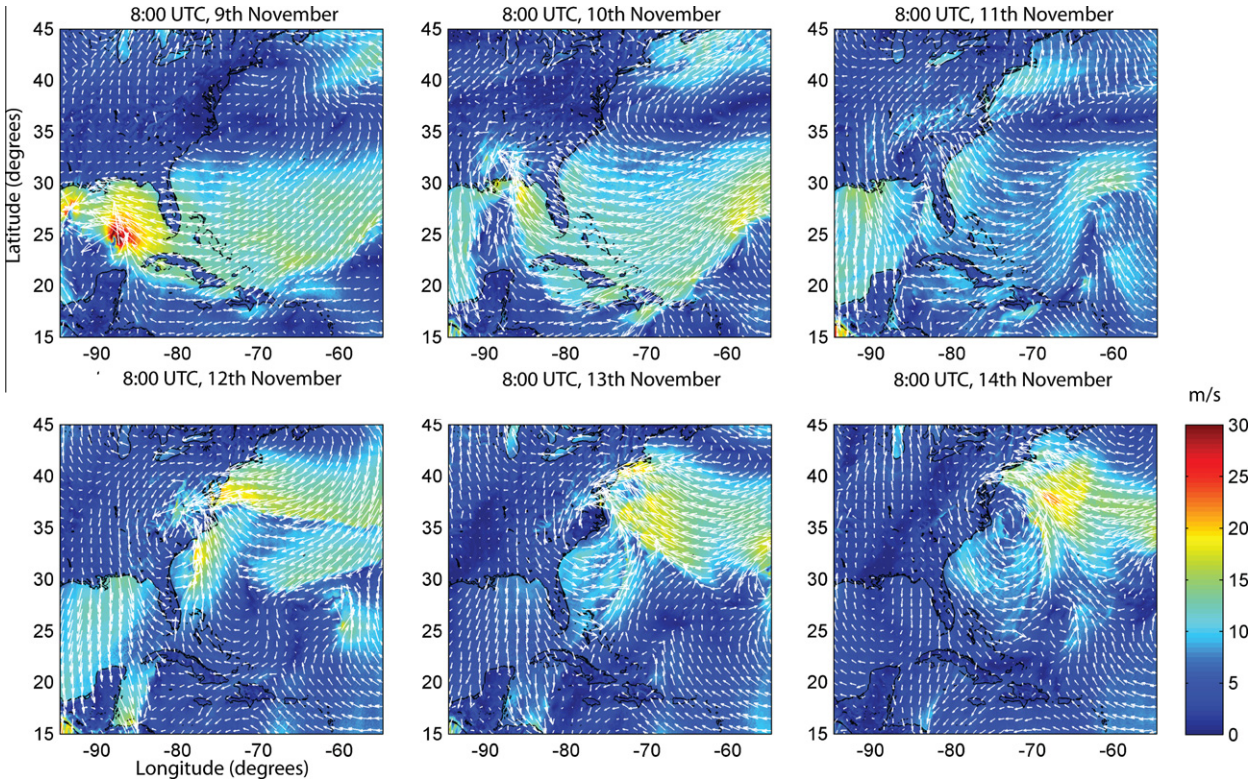

Fig. 4. Wind intensity and direction results from WRF without including the effect of the SST field transferred from ROMS and without the surface roughness transferred from SWAN (run R1).

cyclone during the 2009 Atlantic hurricane season (Avila and Cangialosi, 2010). As it traveled north through the Yucatan Strait, the low pressure system intensified, becoming a Category 2 hurricane (Grosskopf and Bass, 2010). Ida reached its peak wind speed of 46 m s^{-1} over the Yucatan channel at 00:00 UTC on the 9th of November (Avila and Cangialosi, 2010). Thereafter, it moved into the Gulf of Mexico and weakened to a tropical storm, as indicated by data collected from reconnaissance planes and satellite intensity estimates. After 15:00 UTC on the 9th of November, convection redeveloped near the center and Ida once again reached hurricane strength at 18:00 UTC, when it was approaching the mouth of Mississippi river. Ida began to weaken as it moved over cold waters, turned to the northeast and became extratropical a few hours before it moved inland on Dauphin Island, Alabama (12:00 UTC 10th November). In the following days, as a low pressure system developed, it travelled northeastward, reaching an area southeast of Cape Hatteras by the 12th of November. It joined another low pressure system established in that area while an intense anticyclone developed in the northeastern US. The resulting atmospheric pressure gradient generated a coastal storm extending from New England to Cape Hatteras, with strong winds blowing toward the southwest. From November 11–15th, this powerful nor'easter coastal storm, known as Nor'Ida or the "Friday the 13th storm", affected the east coast of the US causing severe flooding, damaging buildings, and eroding beaches. Wind measurements on the 13th of November showed maximum wind speeds up to 23 m s^{-1} along the coast of Virginia. Although Nor'Ida's maximum storm surge values and sustained wind speeds were not as intense as in a hurricane, the storm was one of the most costly in the past two decades and is likely in the top five of the past century (Herrington and Miller, 2010). Persisting for about 5 days, its duration was one of the main factors contributing to its erosion and damage potential.

We applied the COAWST modeling system to investigate atmosphere and ocean dynamics during Hurricane Ida and its evolution into the Nor'Ida storm. One of the most interesting aspects of this event is that it included two different atmospheric extreme conditions, a hurricane and a nor'easter, affecting regions with different oceanographic characteristics. Ida mostly affected the Gulf of Mexico, a microtidal area dominated by the Loop Current and the occasional formation of warm core rings. In contrast, Nor'Ida was established in the region between Cape Hatteras and Cape Cod, a mesotidal area greatly influenced by the Gulf Stream.

The atmosphere–ocean–wave interactions that are examined in this study include the effect of the high resolution ocean SST on the atmospheric module (SST) and the sea surface roughness induced by wind waves (KWS). Although the effects of the sea surface (ELV) and ocean currents (CUR) on the wind wave propagation and generation, the wave forces (VF), the ocean bottom roughness enhancement (KAW), and the turbulent energy injection (TKE) were not analyzed in detail, they were considered in the numerical runs (Table 1). In run R1, WRF did not include the effect of the high resolution SST and the ocean surface roughness was computed using the CHNK formulation. Run R2 added the effect of the high-resolution SST. Runs R3, R4, and R5 added the effect of a specific wave roughness formulation (R3: DGHQ, R4: TY2001, and R5: OOST). In all the numerical runs, winds computed in WRF were used to force SWAN. The heat fluxes and ocean surface stresses computed in WRF represent the atmospheric forcing used in ROMS.

These experiments were intended to investigate how atmosphere–ocean–wave interactions influence wind intensity, atmospheric pressure, storm track, wind waves, sea surface temperature (SST), surface currents, storm surge values, and sea surface stresses. None of these simulations included any type of data assimilation. Our goal was to investigate the variation in the response of the modeling system as different physical interactions were activated. This would be more difficult to ascertain if strong nudging and assimilation methods were introduced.

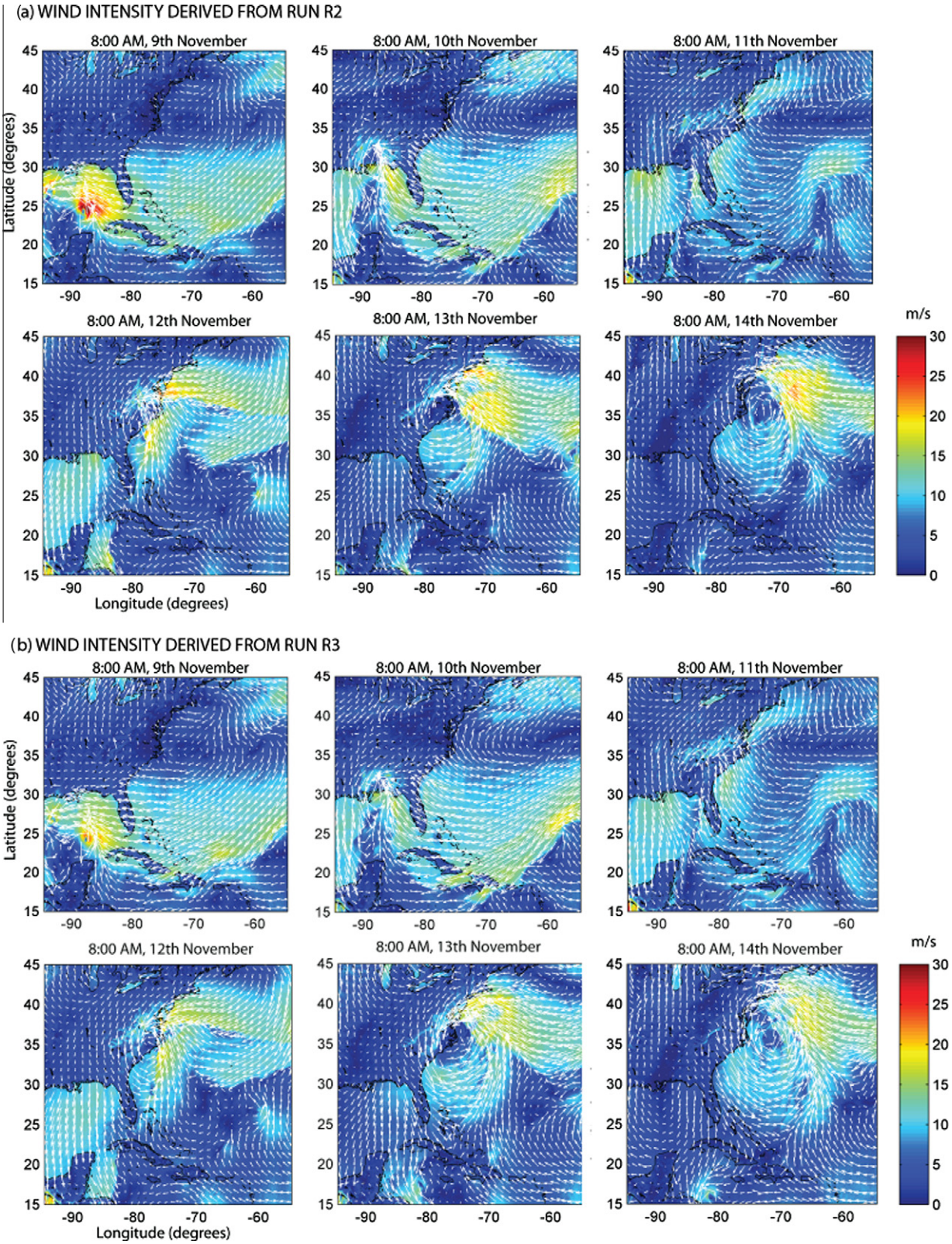

Fig. 5. Wind intensity and direction during the simulation period. (a) Results derived from WRF including the effect of the SST field transferred from ROMS, run R2. (b) Results derived from WRF including the effect of the SST field transferred from ROMS and the surface roughness transferred from SWAN module, run R3.

3.1. Atmospheric field

3.1.1. Wind, pressure and precipitation fields

Fig. 4 shows wind vectors and intensities from the 9th to the 14th of November from WRF with no interaction between the ocean and wave modules (run R1). These results showed the propagation of Hurricane Ida through the Gulf of Mexico from November 9–10th, decreasing in intensity as it traveled towards the northeast on the 11–12th, and strengthening on the 13th as Nor'-Ida developed.

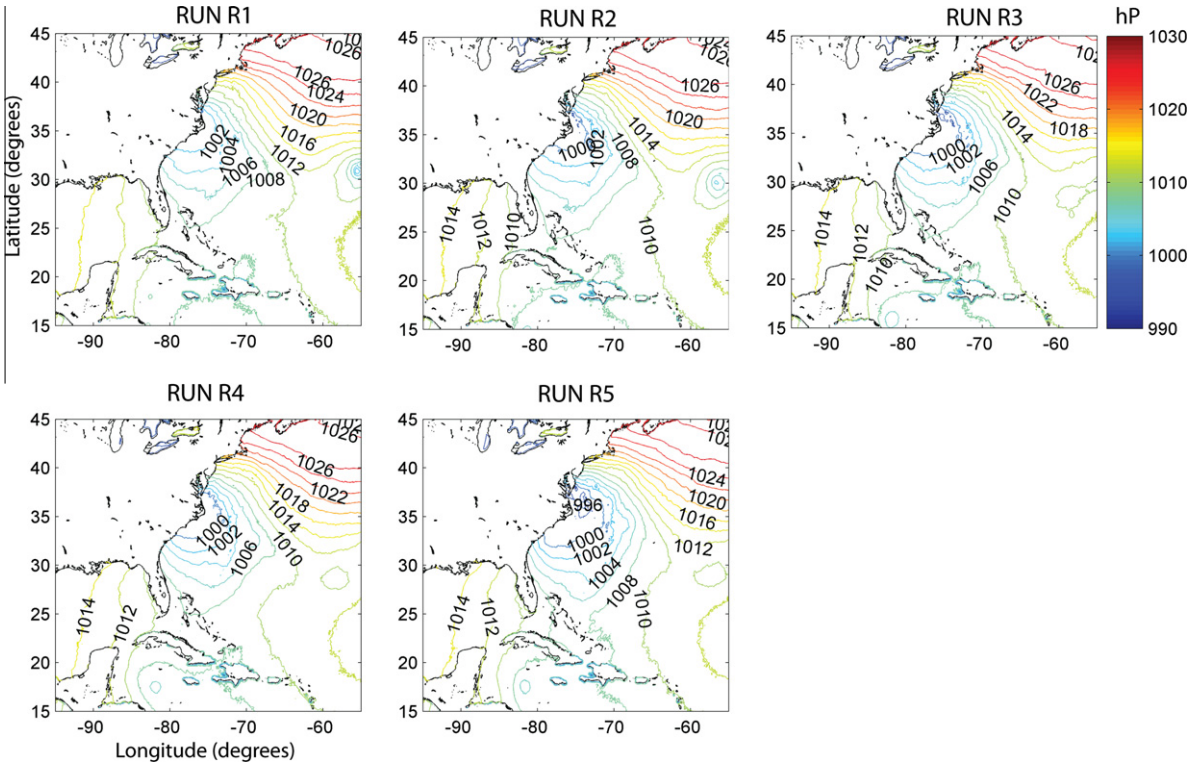

Fig. 6. Spatial distribution of the sea level pressure (hP) computed in runs R1, R2, R3, R4, and R5 the 13th of November at 13:00 UTC.

To test the impact of the high resolution SST and the ocean wave roughness, the results from R1 were compared to the results of the R2, R3, R4, and R5 simulations. Including the high-resolution SST provided by ROMS (R2) did not greatly modify the wind intensity (Fig. 5(a)) during the passage of Ida though the Gulf of Mexico. However, including the effect of wave roughness (R3) reduced the wind strength by 5–10 m s^{-1} (10–25% reduction) (Fig. 5(b)).

During Nor'Ida, the high-resolution SST tended to intensify the winds during the storm peak, while wave-induced ocean roughness played the opposite role. These interactions also modified the position, form, and horizontal extent of the main low pressure cell during Nor'Ida. Considering both interaction processes, the cyclone was stronger and had a larger horizontal extent, with the eye displaced eastwards (Fig. 6). This effect was more noticeable when including the roughness provided by OOST (R5) and less important with DGHQ (R3). The central pressure associated with Nor'Ida decreased by 4 hP because of the ocean roughness in run R5, with minimum values of 996 hP on the 13th of November at 13:00 UTC. These values are in better agreement with the pressure fields provided by the Daily Weather maps from NOAA, which showed a minimum pressure of 994 hP at 13:00 on the 13th of November. Doyle (2002) also identified reductions of 8 and 3 hP in the central pressure in simulations of the tropical cyclones Mitch and Bret, respectively, due to the effect of waves. He observed that this effect was related to the increase of latent heat flux and the consequent increase in rainfall. Perrie and Zhang (2001) coupled a regional climate model to an ocean wave model for the North Atlantic to consider the impact of waves on regional climate simulations. They observed that the atmosphere–wave coupling generated reductions in the sea level pressure near the storm center and enhanced convective precipitation.

As explained by Zhang and Perrie (2001), two main ocean–atmosphere interaction processes affect storm intensification and evolution. In the first, momentum is transferred from the atmosphere to the ocean by the increase of ocean surface roughness due to wind waves. This interaction produces a reduction in surface wind speeds. The second interaction is related to the increase of heat fluxes from the ocean to the atmosphere, resulting in an intensification of the synoptic system. In the case of Nor'Ida, the heat and moisture fluxes were influenced by the wave state through surface momentum flux. In Nor'Ida, the increase of the ocean roughness also produced an increase of sensible latent heat flux and rainfall rates (Fig. 7).

The mean latent and sensible heat fluxes for the period between the 12th and the 13th of November doubled due to both coupling effects (high resolution SST and wave-induced roughness) along the coast of Florida and South Carolina. The increase was also noticeable at South Cape Cod. On November 12th, the remnant of Ida traveled along the coast of Florida and South Carolina. The increase of latent and sensible heat fluxes due to the increase of wave roughness in this area contributed to the intensification of the low pressure system (intensifying the warm core and increasing the water vapor content of the cyclone). On the 13th, the low pressure cell was blocked by a high pressure system located in New England where stopped moving northwards and started to dissipate. The cyclone absorbed more latent heat flux and more water vapor due to the increase of the ocean wave roughness along the coast of South Carolina, resulting in higher precipitation as the system started to dissipate. Because the low pressure system was located more southeastward when including the effect of the waves, the location of the maximum precipitation rates was modified, increasing offshore from Cape Hatteras and displacing the maximum precipitation areas landward towards the coasts of North Carolina and Virginia. The maximum accumulated precipitation over land was measured in Hampton, VA (Lon = −76.34 W, Lat = 37.032 N). When the effect of the ocean roughness was included, the maximum precipitation rates were obtained close to Hampton (Lon = −76.68 W, Lat = 36.81 N); however, without the interaction, this maximum was located in Lon = −78.34 W and Lat = −37.01 N, displaced 220 km landward (Fig. 8). The precipita-

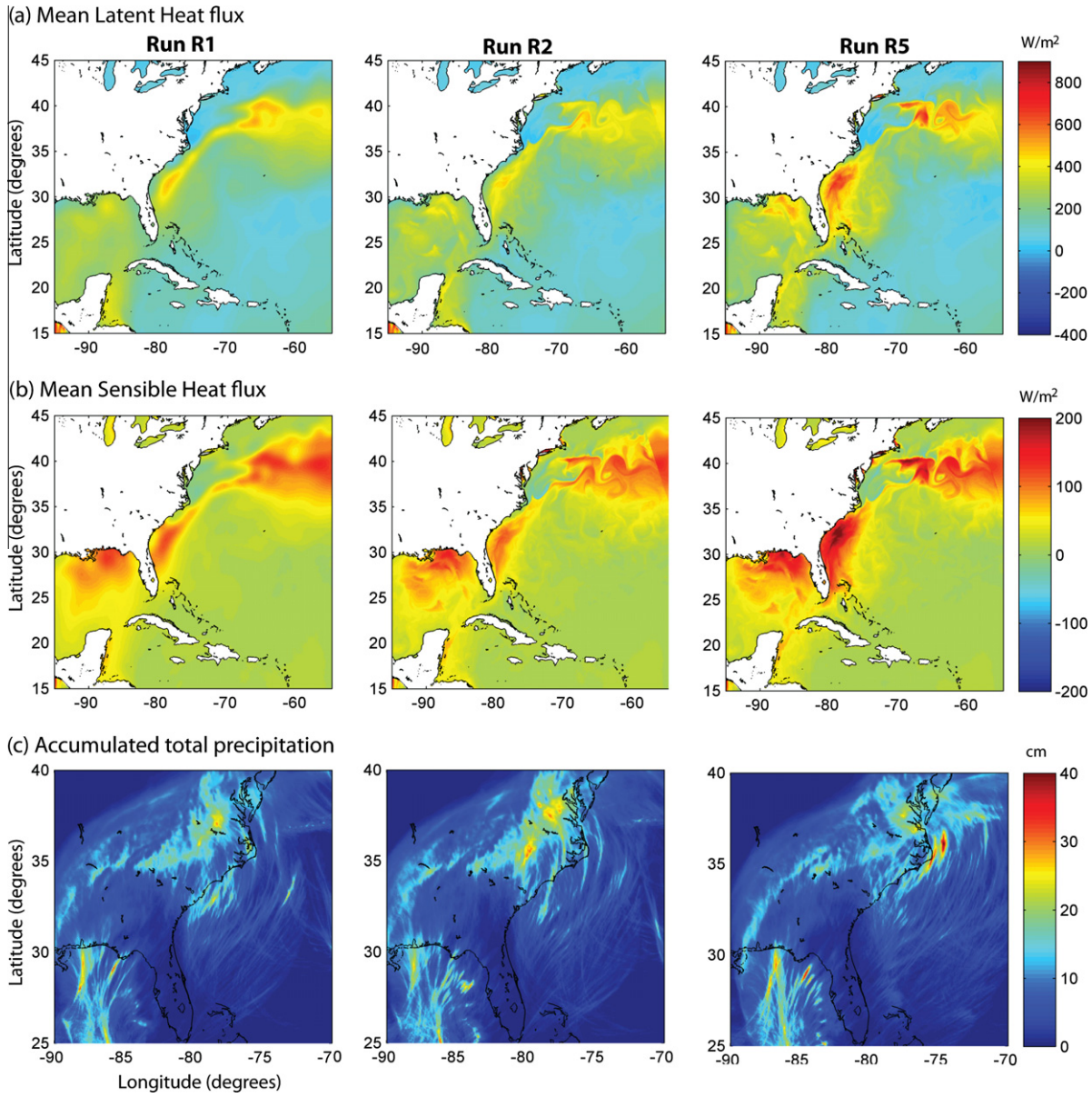

Fig. 7. Spatial distribution of the (a) latent heat flux (W/m^2), (b) sensible heat fluxes (W/m^2), and (c) accumulated precipitation (cm) computed in runs R1, R2, and R5. Latent and sensible heat fluxes are averaged from the 12th to the 13th of November. The accumulated precipitation represents the accumulation during the 10th and the 14th of November.

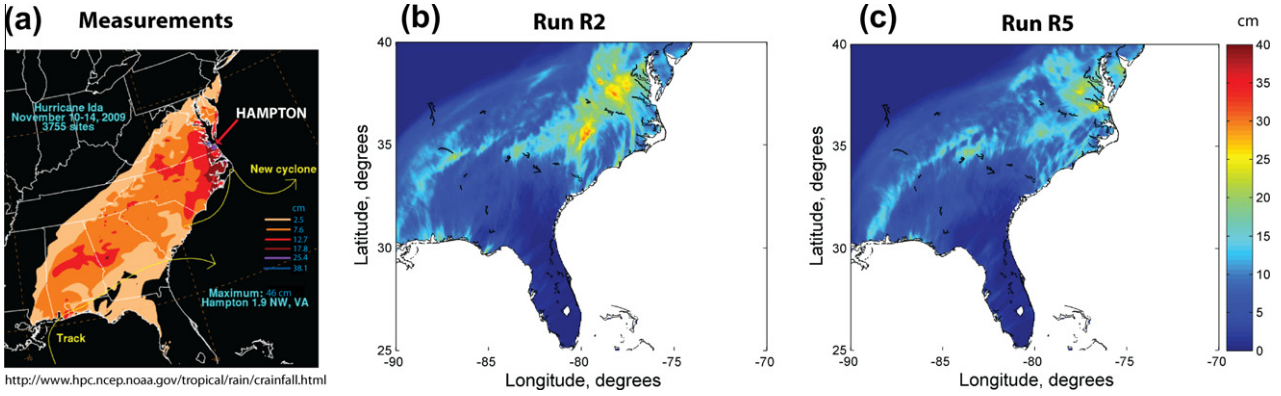

Fig. 8. Comparison between measured and modeled accumulated precipitation over land, from the 10th to the 14th of November, 2009: (a) measured precipitation, (b) simulated accumulated precipitation over land (run R2), (c) simulated accumulated precipitation over land (run R5).

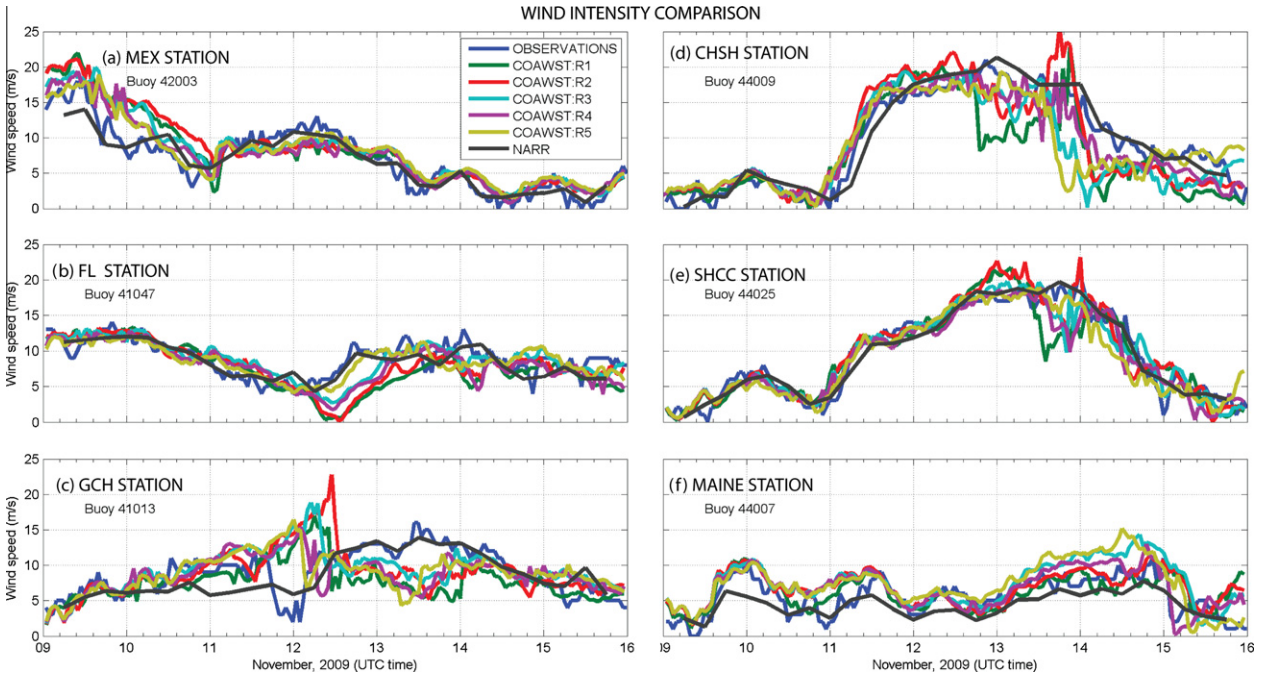

Fig. 9. Comparison of the measured and computed wind intensity time series. Winds derived from the North Atlantic mesoscale model run by NCEP in a forecast system, which includes data assimilation, were also included in the comparison (presented with the black line). The six characteristic stations and regions are shown in Fig 2.

Table 2
Model skill and RMSE in the characteristic stations.

	RMSE (m/s)						Skill					
	MEX skill	FL skill	GCH skill	CHSH skill	SHCC skill	MAINE skill	MEX RMSE	FL RMSE	GCH RMSE	CHSH RMSE	SHCC RMSE	MAINE RMSE
R1	3.24	3.16	4.78	3.91	2.9	2.28	0.74	0.74	0.26	0.91	0.93	0.76
R2	3.41	2.95	4.91	3.2	1.96	2.59	0.71	0.75	0.3	0.95	0.97	0.67
R3	2.87	2.21	4.3	3.29	1.83	2.56	0.78	0.82	0.35	0.94	0.97	0.72
R4	2.62	2.28	4.37	2.3	2.05	2.58	0.79	0.82	0.29	0.97	0.97	0.69
R5	2.26	1.54	4.41	3.78	1.37	2.68	0.85	0.9	0.31	0.92	0.99	0.68
NAM	1.53	1.35	2.36	2.05	1.39	2.89	0.92	0.92	0.85	0.98	0.99	0.58

tion also increased on the sea side, offshore from Cape Hatteras, due to the ocean wave roughness.

To further investigate the effects of the model coupling, the computed wind speeds were compared to the winds measured from NDBC buoys. Given the number of buoys considered, it was not feasible to show all of them. Therefore, the study domain was divided into 6 regions with different meteorological and oceanographic characteristics. A representative station was chosen for each domain. In Fig. 2(a), the extension or coverage of the considered domains, together with the location of the selected stations, are shown. The domains are the Gulf of Mexico (MEX), the east coast of Florida (FL), the coast of Georgia north to the southern Outer Banks of North Carolina (GCH), the coastal zone between Cape Hatteras and Sandy Hook (CHSH), the area from Sandy Hook to Cape Cod (SHCC) and the Gulf of Maine (MAINE).

A comparison of wind speed data at each station is shown in Fig. 9. The model skill (S) (computed with the skill factor proposed by Wilmott (1981)) and the root mean square error (RMSE) for each selected station are indicated in Table 2. The top left panel in Fig. 9 shows the intensity in the Gulf of Mexico. The first wind intensity peak, occurring on the 9th of November, indicates the passage of Hurricane Ida with the highest wind intensities of the simulation period. All stations affected by the passage of Ida showed that if the effect of the ocean roughness was not included (R2), the computed winds in the Gulf of Mexico during the passage of Hurricane Ida were too strong. The high-resolution SST did not produce significant variations. With the inclusion of the enhanced wave roughness, the maximum wind intensities were reduced and the COAWST's model skill increased considerably. In general, the best agreement with the measurements was obtained in run R5, with model skill values lower but close to those obtained with NARR, noting that NARR assimilates data, whereas we do not.

In contrast to the reduction of wind speed identified during the passage of the hurricane, at the FL (located off the coast of Florida) and MEX stations on the 12th and 13th of November, the inclusion of ocean roughness created an increase in the wind speed. The ocean surface pressure analysis showed that the ocean wave roughness intensified and enhanced the main low pressure cell located in Cape Hatteras. As a result, winds associated with this cyclone had a larger horizontal extent, increasing the wind intensity in the east of the Gulf of Mexico and off the Florida coast. The better agreement with the measured data indicates that the extension and intensity of the winds in this area are modeled more accurately when the ocean roughness is included.

At the GCH station, during the Nor'Ida peak, an unrealistic sudden wind intensity change occurred if the roughness effect was not included (red and green lines). This jump in the wind speed was reduced with ocean roughness inclusion, but the model skill was still poor. Between the 11th and the 14th of November, the CHSH and SHCC stations showed an intense wind event during the development of Nor'Ida. At SHCC, the wind intensities provided by COAWST agreed with the measurements and had skill values higher

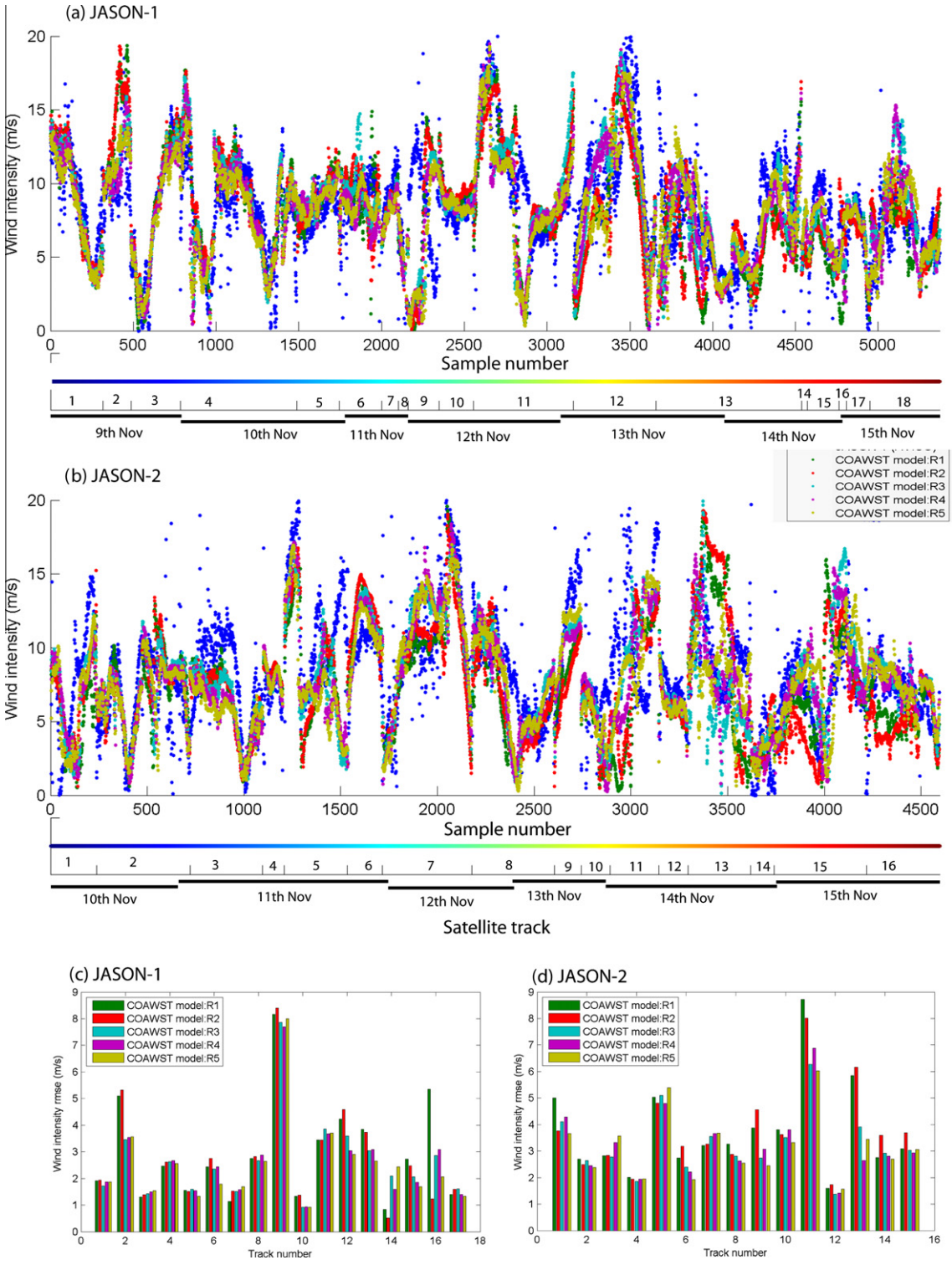

Fig. 10. Measured and computed wind intensities along the satellite track: (a) JASON-1 data, (b) JASON-2 data.

than 0.90. At CHSH, as well as at MAINE, the enhancement of the roughness resulted in a reduction of the skill. In the case of MAINE, the proximity of the boundary conditions could affect modeled winds. It is interesting that even though the TY2001 and DGHQ closure models are based on different wave parameters (wave steepness and wave age, respectively), the computed wind intensities were similar with both models. In general, the OOST model (yellow lines) produced better agreement with the measurements. The spatial variation of the model skill for the different experiments (not shown) indicated that if the effects of the high-resolution SST and wave roughness were not considered in WRF (run R1), the model skill was smaller than in runs R2 and R5. Run R5 showed the highest skill, and the high-resolution SST did not generate significant changes in the model's skill.

The quality of wind speed prediction in the offshore region was analyzed by comparing modeled wind intensities with measurements from the JASON-1 and JASON-2 satellites. For each satellite measurement, the closest model data point (both in the space and

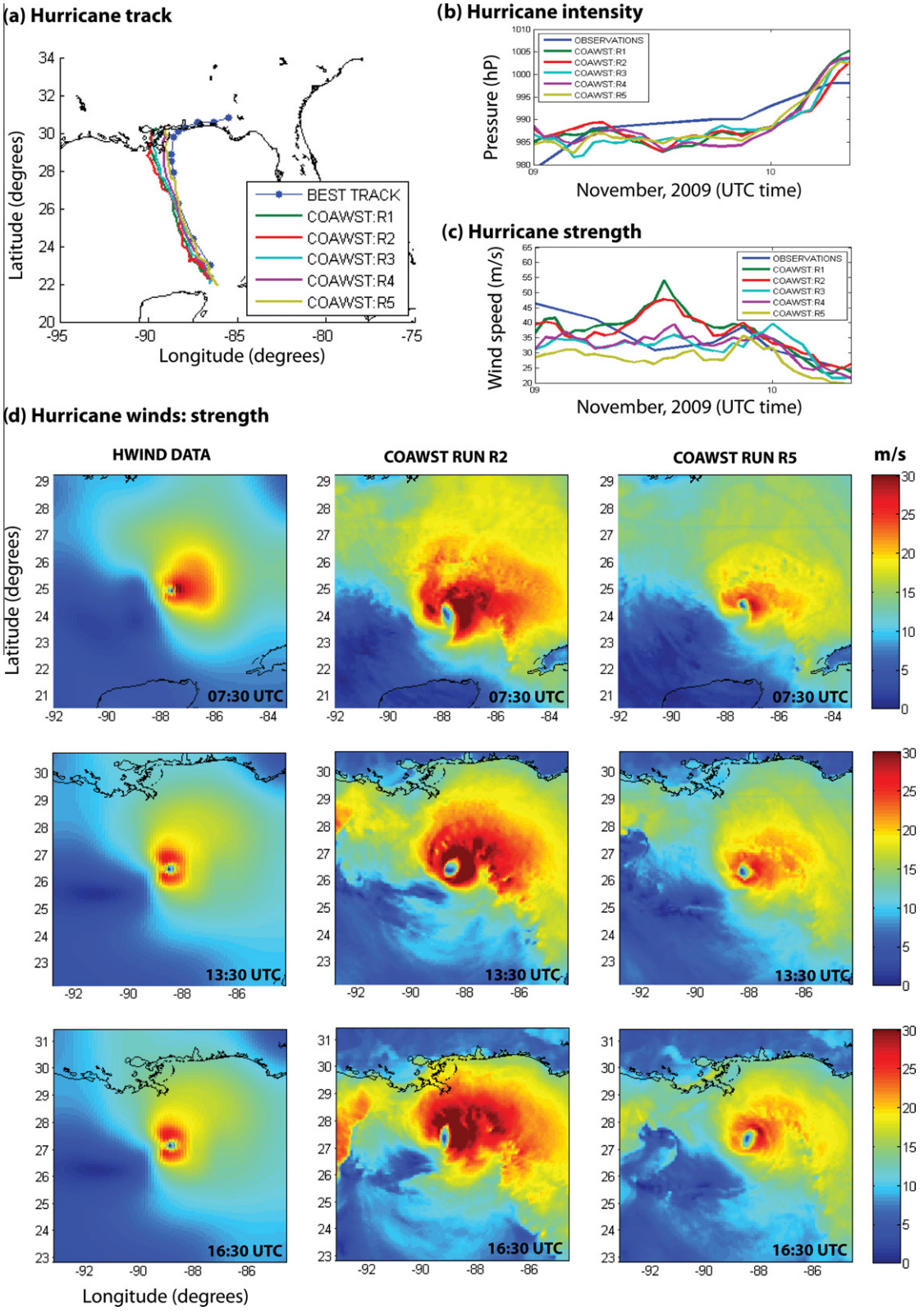

Fig. 11. Hurricane Ida. Comparison of the computed hurricane and values reported in the Tropical Cyclone Report for Hurricane Ida (in blue): (a) tracks, (b) minimum atmospheric pressure, (c) maximum wind speed and (d) comparison of the Surface Wind Analysis (Hwind) data and modeled wind fields. (For interpretation of the references to colour in this figure legend, the reader is referred to the web version of this article.)

in time) was computed. Fig. 10 shows the comparison of the measured and computed wind intensities for each satellite sample. Panel (a) shows the JASON-1 data comparison; the top graph represents the data comparison, with the lines in the bottom indicating the corresponding track (the color indicates the track shown in Fig. 3, and the number below the line indicates the track number). Panel (b) shows the same comparison but with the JASON-2 satellite measurements. The bottom plots depict the RMSE (root

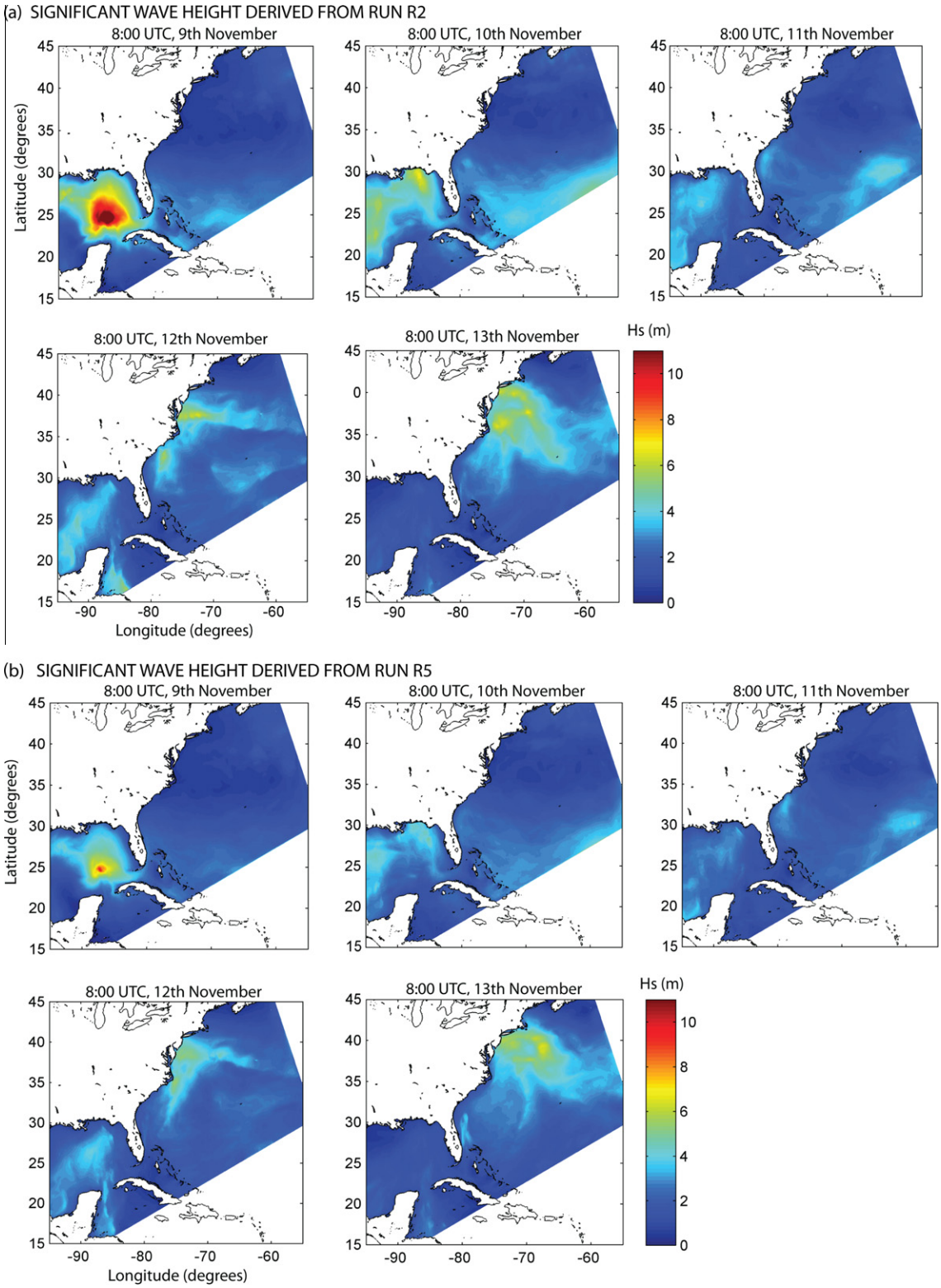

Fig. 12. Spatial distribution of significant wave height: (a) run R2 and (b) run R5.

mean square error) between measurements and the computed wind intensities for each satellite, as well as the individual track and each numerical run.

In general, the RMSE between the measurements and the numerical results was between 2 and 4 m s^{-1}, indicating a good agreement between the model and the measurements. However, some periods in which the results differed from the measurements were identified. The RMSE in most of the JASON-1 tracks was between 1 and 3.5 m s^{-1}. On November 12th, the RMSE increased up to 6 m s^{-1} in all of the numerical runs, when the model was not able to reproduce an intense wind event that was observed in the Western Gulf of Mexico. Including sea surface roughness

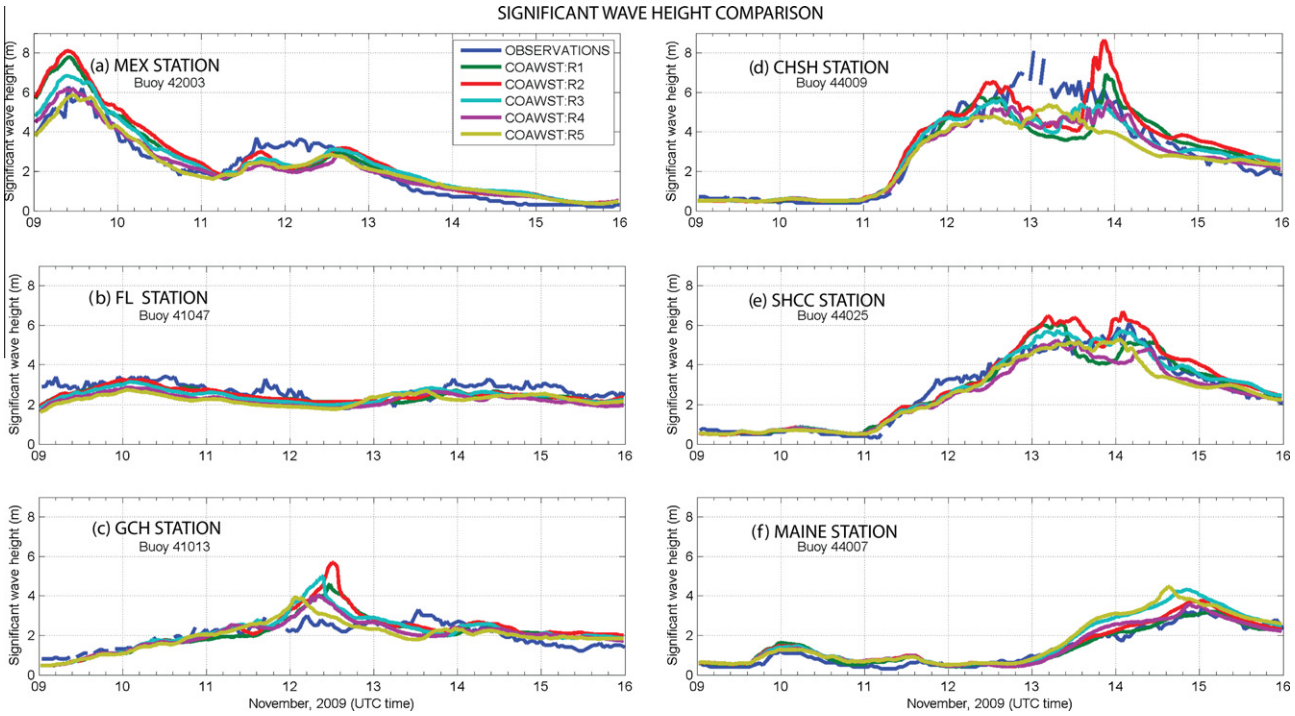

Fig. 13. Comparison of the measured (blue) and computed significant wave height time series at different stations. (For interpretation of the references to colour in this figure legend, the reader is referred to the web version of this article.)

Table 3
Model skill in the characteristic stations.

	RMSE (m)						Skill					
	MEX skill	FL skill	GCH skill	CHSH skill	SHCC skill	MAINE skill	MEX RMSE	FL RMSE	GCH RMSE	CHSH RMSE	SHCC RMSE	MAINE RMSE
R1	0.7	0.43	0.74	1.63	0.74	0.33	0.92	0.75	0.66	0.87	0.96	0.88
R2	0.78	0.41	0.87	1.71	0.96	0.34	0.91	0.76	0.62	0.88	0.94	0.87
R3	0.63	0.48	0.75	1.19	0.73	0.46	0.93	0.69	0.68	0.93	0.96	0.84
R4	0.61	0.56	0.63	1.28	0.67	0.37	0.93	0.61	0.71	0.92	0.96	0.86
R5	0.53	0.62	0.62	1.13	0.69	0.49	0.94	0.49	0.7	0.93	0.96	0.83

did not change or improve the wind intensity estimation for most of the individual tracks. The most significant reduction of the RMSE produced by the ocean roughness was observed for those data measured on the outer shelf region close to Cape Cod on the 14th of November. However, the wind speeds modeled on the 14th of November were lower than the measurements. The observed discrepancies may also be derived from inaccuracies in the empirical model used to derive the wind intensity data, as previously discussed. Corroborating the previous observations, the comparison showed that including sea surface roughness led to better agreement between the measurements and the numerical results. However, it is difficult to ascertain which surface roughness closure model provides the most accurate results.

The results indicate that the observed wind speeds, as well as the low pressure cell changes, during Nor'Ida were mainly a consequence of the ocean wave surface roughness inclusion, which affects both the momentum flux transfer and the heat fluxes. In general, the roughness effect was more noticeable during the passage of Ida, when the wind speeds reached their maximum values.

3.1.2. Hurricane Ida

In this section, the specific characteristics of Hurricane Ida, such as its track, strength, and intensity, are analyzed. Fig. 11(a) shows the best track reported in the Tropical Cyclone Report (Hurricane Ida) for the period between the 9th and the 11th of November along with tracks computed by the different numerical experiments.

As in Warner et al. (2010), the hurricane tracks (Fig. 11(a)) did not significantly differ between the runs, and in general, they agreed with the observed track. This is in agreement with Marks and Shay (1998), who asserted that large-scale processes determine the tropical cyclone track forecast, and not mesoscale processes influenced by ocean coupling. However, prior to landfall in front of the Mississippi Delta, all of the tracks deviated westwards from the observations. This deviation was more severe in runs R1, R2 and R3, while R4 and particularly R5 showed a better agreement with the measurements. The insensitivity of the hurricane track to the ocean wave roughness parameterization in the offshore region agrees with previous work (e.g., Doyle, 2002). However, in the region close to the coast, the differences were noticeable, producing changes of up to 100 km in the landfall location.

In all cases, the sea level pressure was underestimated by between 5 and 7 hP along the track (Fig. 11(b)), while the hurricane strength was overestimated when the ocean roughness was estimated using the CHNK closure (Fig. 11(c)). The comparison of the wind field evolution (shown in Fig. 11(d)) for the different numerical experiments demonstrated a high sensitivity to the ocean surface roughness. The comparison with Surface Wind Analysis data

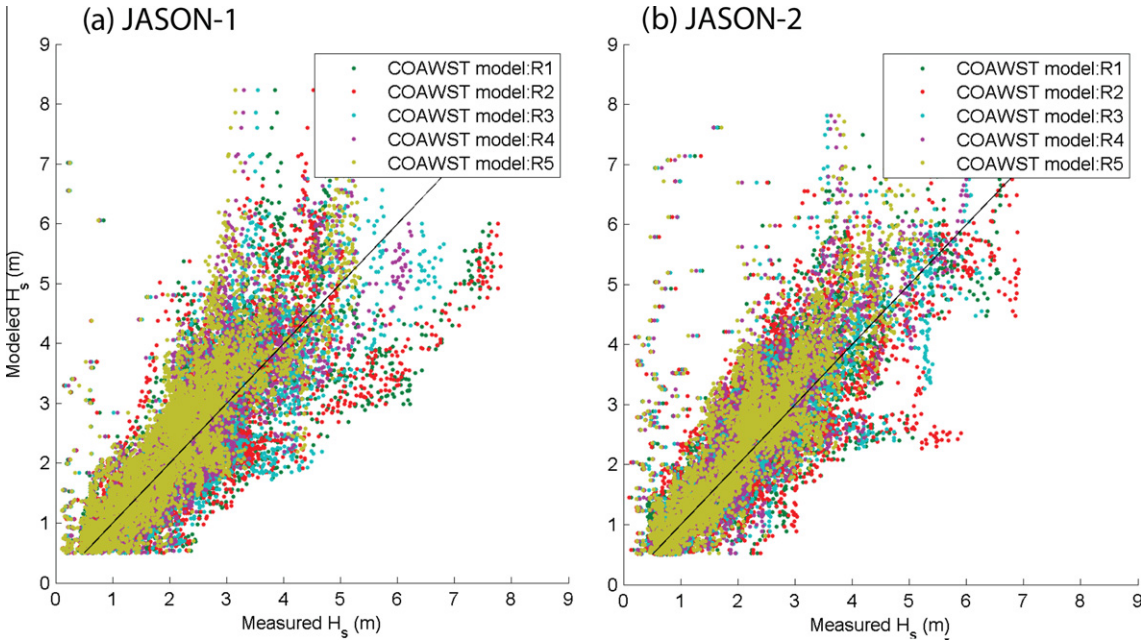

Fig. 14. Significant wave height scatter plot, comparison between model simulations and JASON-1 and JASON-2 altimeter data.

from the Hurricane Research Division of NOAA showed that without considering the roughness effect, the modeled hurricane was too strong (10–15 m s^{-1} over-estimation) and asymmetric. The dimension of the warm core, as well as the extension of the wall, was reduced with the increase of the ocean roughness (more intense with OOST closure than with DGHQ and TY2001). The high-resolution SST and the wave roughness enhanced the ocean-to-atmosphere latent and sensible heat fluxes (not shown). The average maximum latent heat flux between the 9th and 10th of November increased from 500 W/m^2 in run R1 to 612 W/m^2 due to the high-resolution SST in run R2 and to 713 W/m^2 in run R5. This would intensify the cyclone if the increase of the momentum flux had a lower impact on decelerating the atmospheric motion.

3.2. Wave field

One of the direct consequences of wind blowing over the ocean is the energy or momentum transfer from the atmosphere to the water, which generates wind waves. As mentioned by Zhang and Perrie (2001), without waves, atmospheric momentum would pass directly into ocean currents. However, because of this interaction, some of the momentum goes into waves, while some is transferred to surface currents and some is radiated away from the generation area by wave propagation. The maximum wave height that develops during a given storm is dependent on the wind intensity, as well as the storm duration and spatial coverage. Large geographical fetch and longer temporal durations result in an increased sea state, with waves characterized by longer periods and higher wave heights.

During the analyzed period, two different conditions of wave development were identified. The first corresponds to the rapid passage of Hurricane Ida along the Gulf of Mexico. Because Ida was moving fast, passing through the Gulf of Mexico in less than 32 h, the wind wave generation zone was restricted to the hurricane area. However, these winds were intense (between 35 and 40 m s^{-1}) and generated waves with significant wave heights up to 7 m and peak periods of 12.5 s. In contrast, Nor'Ida produced intense southwestward winds between Cape Cod and Cape Hatteras, with maximum gust intensities of about 23 m s^{-1}. Although these winds were not as intense as those observed during Ida, the wind blew for approximately 4 days over a larger area, resulting in significant wave heights of up to 8 m and 15 s peak periods, as observed between Cape Hatteras and the coast of Virginia. Fig. 12 shows the spatial distribution of significant wave heights in (a) run R2 and (b) run R5 for different periods during the Ida-Nor'Ida event. Two different significant wave height maxima can be observed. One represents waves generated during the passage of Ida thru the Gulf of Mexico (9th of November), and the second represents those generated during the nor'easter (13th of November). Notice the intense significant wave height reduction induced by the ocean surface roughness, especially in the Gulf of Mexico at 8:00 UTC on the 9th of November and also during the Nor'Ida peak. The reduction in surface wind speeds and consequently in wave height is consistent with earlier atmosphere–wave numerical experiments (Webber et al., 1993; Doyle, 1995; Janssen and Viterbo, 1996; Lionello et al., 1998; Desjardins et al. 2000; Zhang and Perrie, 2001; Doyle, 2002; Warner et al., 2010).

Comparing model wave heights to measurements at the 6 selected stations (Fig. 13) showed that, between the 9th and the 10th, all stations except MEX had low waves. The MEX station was impacted by the hurricane on November 9th, resulting in a 6 m peak. After the 11th, the impact of the nor'easter was noticeable at the other stations, especially at CHSH and at SHCC. Including ocean roughness reduced the maximum significant wave height by up to 2 m at some of the stations at the peak of the storms. This effect was especially noticeable at MEX, CHSH and SHCC. The choice of sea surface roughness parameterization led to a 1 m difference in the maximum significant wave height. The OOST closure model produced the highest reduction of the wind intensity and therefore the smallest wave heights. The differences between TY2001 and DGHQ were smaller than those obtained with respect to OOST. In general, the OOST parameterization (R5) yielded model results that were the closest to the observed values.

The RMSE and the model skill for each model run and each characteristic station are given in Table 3.

The root mean square error at all stations decreased by about 0.4 m when the ocean surface roughness at the stations in the MEX region was included. The lowest RMSE and the highest skill values were obtained for run R5.

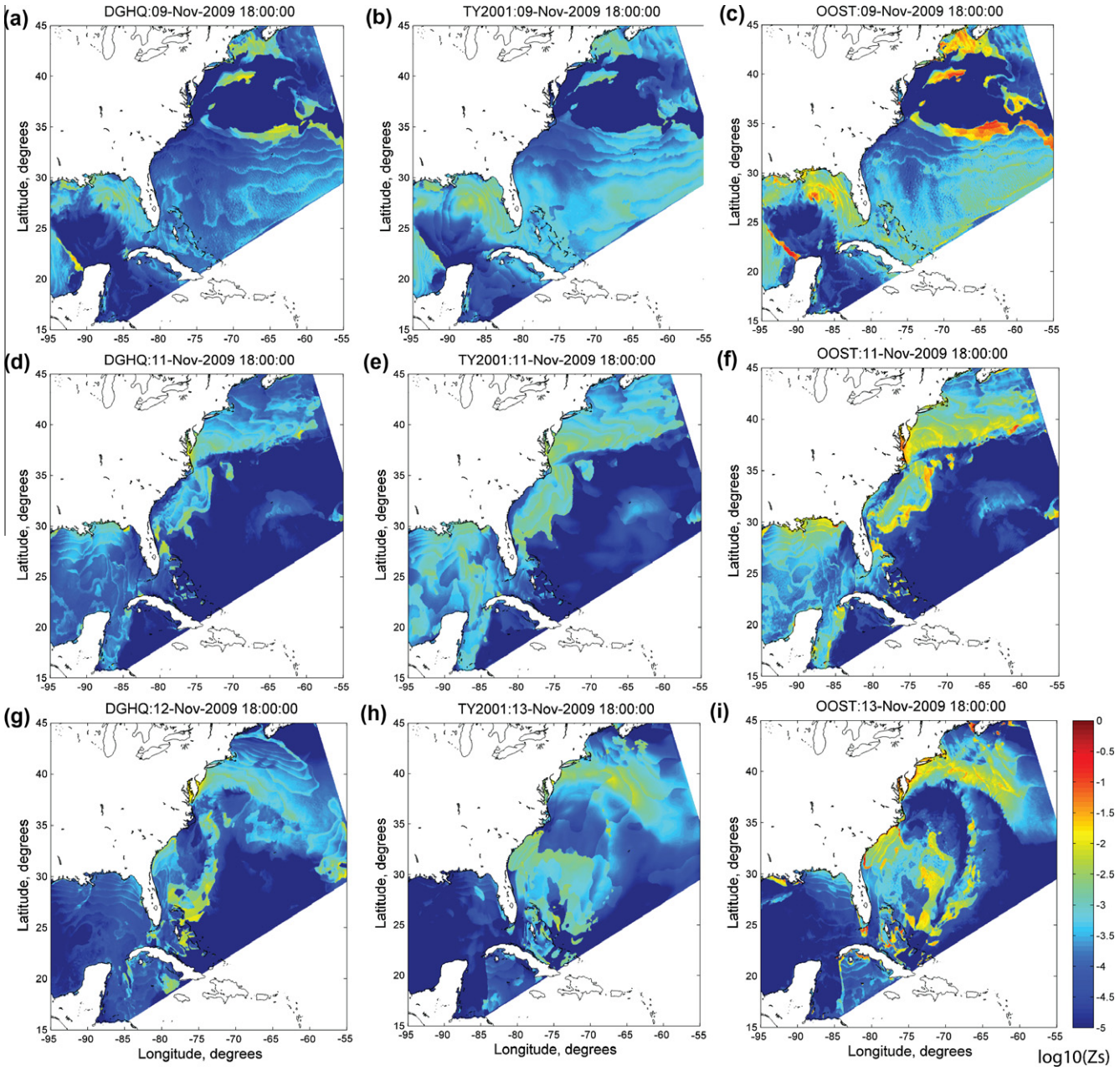

Fig. 15. Spatial distribution of the sea surface roughness (log scale) given by DQGH, TY2001, and OOST at several time instants.

Comparing the simulated significant wave heights to the JASON-1 and JASON-2 *Ku band* significant wave height data, a high correlation with the measurements was obtained for all numerical runs. However, when only the effect of the high-resolution SST was considered, an over-estimation of the significant wave height resulted along of the tracks, producing an increase of the RMSE. This wave growth over-estimation was a consequence of the high wind speeds computed when the effect of the sea surface roughness was not considered. When the effect of the wave-enhanced ocean roughness was considered, the RMSE varied between 0.2 and 1 m depending on the track and the numerical run. Plots of measured vs. modeled values (see Fig. 14) demonstrated that in both R1 and R2, the high significant wave heights were overestimated. This overestimation, as well as the data dispersion, was reduced when introducing the effect of the ocean surface roughness, as shown by the reduced scatter for R5. The observed data dispersion (note the increase with the wave height) could be related to the spatial resolution of the model, the frequency of the model result storage, the accuracy of the model in different regions, and the accuracy of the method used to infer the wave heights from the altimeter data. The results obtained by considering the OOST closure model showed a smaller scatter and a better fit to the diagonal, suggesting that this closure model was more suitable for the present application than DGHQ or TY2001. However, the differences are not significant.

3.3. Ocean surface roughness

The ocean roughness affects the dynamics of the atmospheric boundary layer by reducing the sea level wind speed and therefore the wave growth, as well as by increasing the heat and moisture fluxes from the atmosphere to the ocean. Fig. 15 shows the spatial

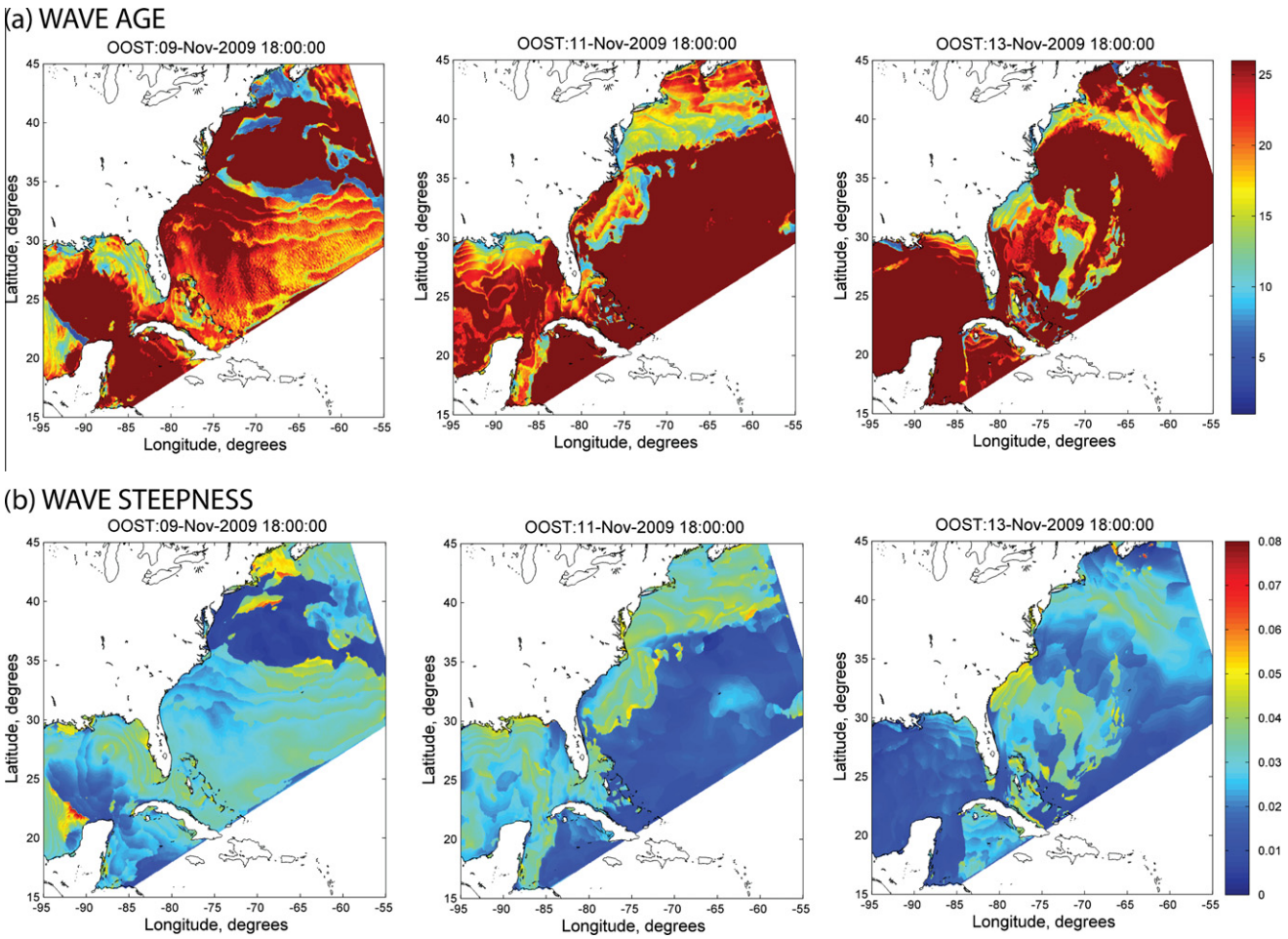

Fig. 16. Spatial distribution of (a) wave age and (b) wave steepness given by OOST at several time instants during the simulation period.

and temporal variation of the sea surface roughness (note log scale) for the three considered closure models. In all cases and depending on the wave characteristics, the surface roughness showed spatial variations of several orders of magnitude. Although the spatial distribution showed similar patterns between the models, differences of several orders of magnitude were observed in areas with the most energetic waves. In all cases, the OOST model provided the highest ocean surface roughness. Because OOST considers the effect of wave steepness and wave age, it represents a roughness field that merges those variations observed in DGHQ (which only considers the effect of the wave age) and those in TY2001 (which depends on wave steepness).

However, it is important to consider that wave age and steepness are not independent parameters. As explained by Lionello et al. (1998), if the wind was blowing in a steady direction and constant speed over an infinite distance, the generated waves would become progressively higher, longer, and less steep. In this case, the waves would progressively get older. Because the sea surface roughness is higher for young waves, the roughness would progressively decrease. However, the pattern of wave development in a real storm is complex. In real situations, due to the spatial and temporal variation of wind vectors, wind continually generates new waves and stops acting on those traveling out of the storm. Fig. 16 depicts the spatial distribution of the wave age and wave steepness computed in run R5, showing the high correlation between both parameters. The youngest waves are also the steepest waves. The comparison of wave age, steepness, and roughness fields during the same time periods (Fig. 15(c), (f) and (i)) shows that the steepest and youngest waves produced the highest ocean roughness areas. On November 11th, the region between East Florida and South Carolina was characterized by particularly young and steep waves, enhancing the effect of the ocean roughness by increasing heat and moisture fluxes and intensifying the cyclone as previously described.

3.4. Hydrodynamic field

3.4.1. Sea surface temperature (SST)

Fig. 17 compares sea surface temperatures determined at 6 km resolution from the NOAA Geostationary series of satellites (GOES), the ROMS model simulation R4, and the lower resolution RTG-SST data used by WRF if high-resolution SST from ROMS was not activated (run R1). Due to intense cloud coverage during the storm, there were few instances in which the SST data from the satellite measurements could be used for comparison, including the 9th of November (18:00 UTC) (top row) and the 16th of November (21:00 UTC) (bottom row).

On November 9th, before Nor'Ida formed, the SST fields provided by COAWST and RTG-SST (Fig. 17(a)–(c)) correctly reproduced the SST front position between Cape Hatteras and Cape Cod. However, due to the COAWST's higher resolution, this model was able to reproduce, with higher accuracy, the cold water core observed more to the east, as well as the filaments and meso-scale structures associated with the Gulf Stream. Differences were also visible south toward the Bahamas, where the temperature estimated by COAWST was closer to that observed by GOES, with

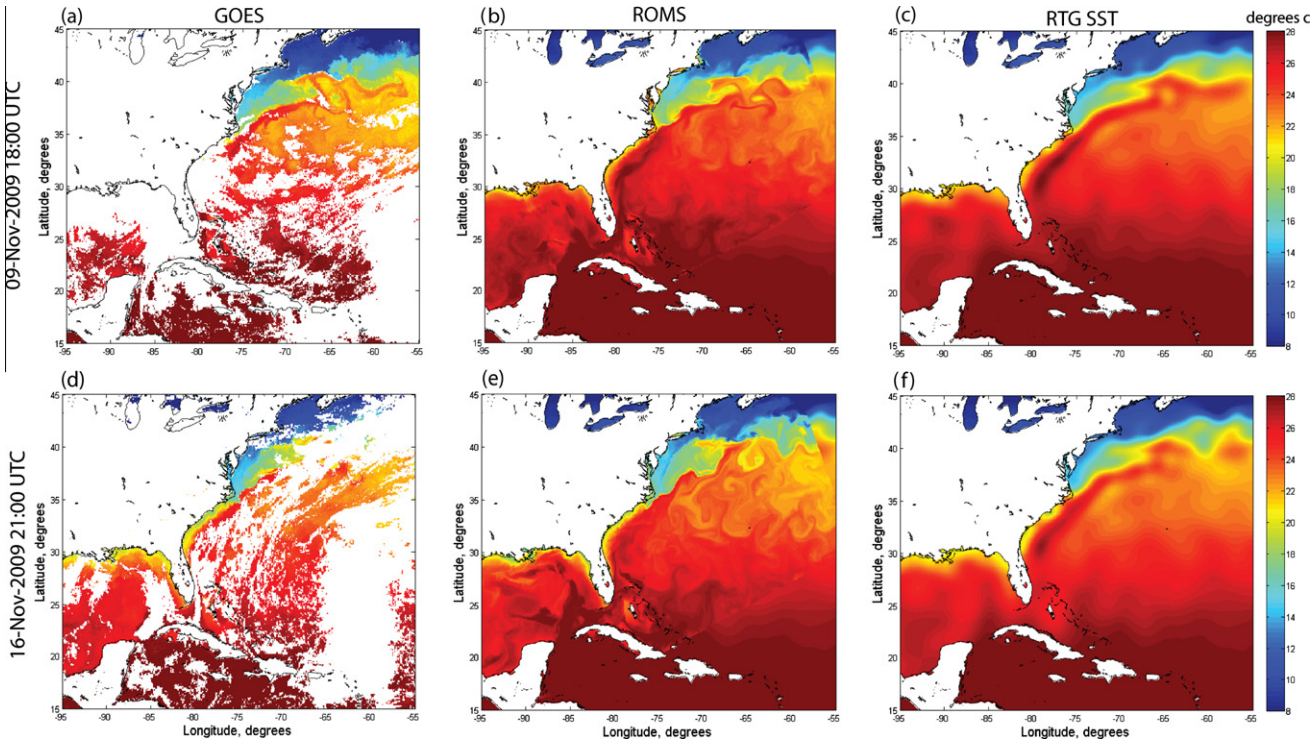

Fig. 17. Comparison of (a) sea surface temperatures at 6 km resolution from the NOAA Geostationary series of satellites (GOES), 9th of November, 2009; (b) high resolution SST provided by ROMS (run R4), 9th of November, 2009; (c) SST given by RTG SST, 9th of November, 2009; (d) sea surface temperatures at 6 km resolution from the NOAA Geostationary series of satellites (GOES), 16th November, 2009; (e) high resolution SST provided by ROMS (run R4), 16th of November, 2009; (f) SST given by RTG SST, 16th of November, 2009.

RTG-SST data overestimating the temperature. After Nor'Ida (Fig. 17(d)–(f)), the temperature front defining the limit of the Gulf Stream became more meandering, a feature reproduced by COAWST. The GOES SST data also showed that the filament structure in the region between Cape Hatteras and Cape Cod after the storm was more defined due to the intrusion of warm water into the shelf region. COAWST captured this overall structure. Another effect of Nor'Ida that can be identified in the GOES images is the displacement of the Gulf Stream northeastwards near Cape Hatteras. This effect, as will be explained in the following section, was caused by the strong wind-driven southwestward flowing surface currents during Nor'Ida. This was captured by COAWST, but the eastward displacement was underestimated.

3.4.2. Surface currents

Three-hour averaged CODAR data for November 2009 were used to estimate the wind-driven and surface currents in the study area. Before Nor'Ida, the daily mean average currents flowed southwestwards in the shelf region between Cape Cod and Cape Hatteras at 0.4 m s^{-1} (see Fig. 18 left panels). The Gulf Stream was close to Cape Hatteras, with mean current velocities of 1.4 m s^{-1}. As the storm developed and intensified, the wind driven surface currents became stronger, with mean values between 0.6 and 0.8 m s^{-1} on November 12th, and the Gulf Stream was still identifiable off of Cape Hatteras.

The maximum surface current intensities were reached on the 13th of November, with values up to 1 m s^{-1} in the North Carolina coastal area. These surface currents displaced the Gulf Stream eastwards and reduced its intensity. On November 14th, the decrease in wind speed led to a weakening of currents (with mean values of about 0.5 m s^{-1}, still flowing southeastwards). However, although the surface currents were not as strong as they had been during the previous days, and the location of the Gulf Stream was still displaced from its original location.

Fig. 18 (right panels) shows the computed daily mean average surface currents in run R4 using Kirby and Chen's (1989) formulation. As explained by Stewart and Joy (1974) and by Kirby and Chen (1989), when currents are not vertically uniform, the dispersion relation of gravity waves is dependent on the vertical current shear. CODAR currents are derived based on the Doppler Effect, and they represent those currents averaged over the depth that affects the wave propagation. For shallow water waves, currents over the entire water column affect wave dynamics, while in deep water waves, near-surface currents have a stronger impact on wave propagation. The formulation given by Kirby and Chen (1989) considers the effect of the relative water depth. On the other hand, in models such as ROMS, the thickness of the grid layers are dependent on the total water depth and can vary significantly between the shallow and the deep depending on the vertical stretching used in the model configuration. The thickness of the grid layers becomes thinner as the depth decreases. Therefore, the current fields of the upper layer represent different vertical levels.

In general, the mean behavior of the ocean surface currents was captured by the model. An increase of current intensity on the shelf was detected as the storm intensified. Current profiles in the shelf region showed a logarithmic vertical profile, indicating that the water column was well mixed. The modeled Gulf Stream intensity near Cape Hatteras was not as intense as that observed in the CODAR data. Because the location of the Gulf Stream and its intensity are determined by the position of the temperature and salinity fronts in that area, the observed differences suggested that the Gulf Stream intensity is off from the start, indicating a poor initial condition. The Gulf Stream partially weakened the southward currents offshore of Cape Hatteras in both the model and the observed data. Some localized differences between measurements and numerical

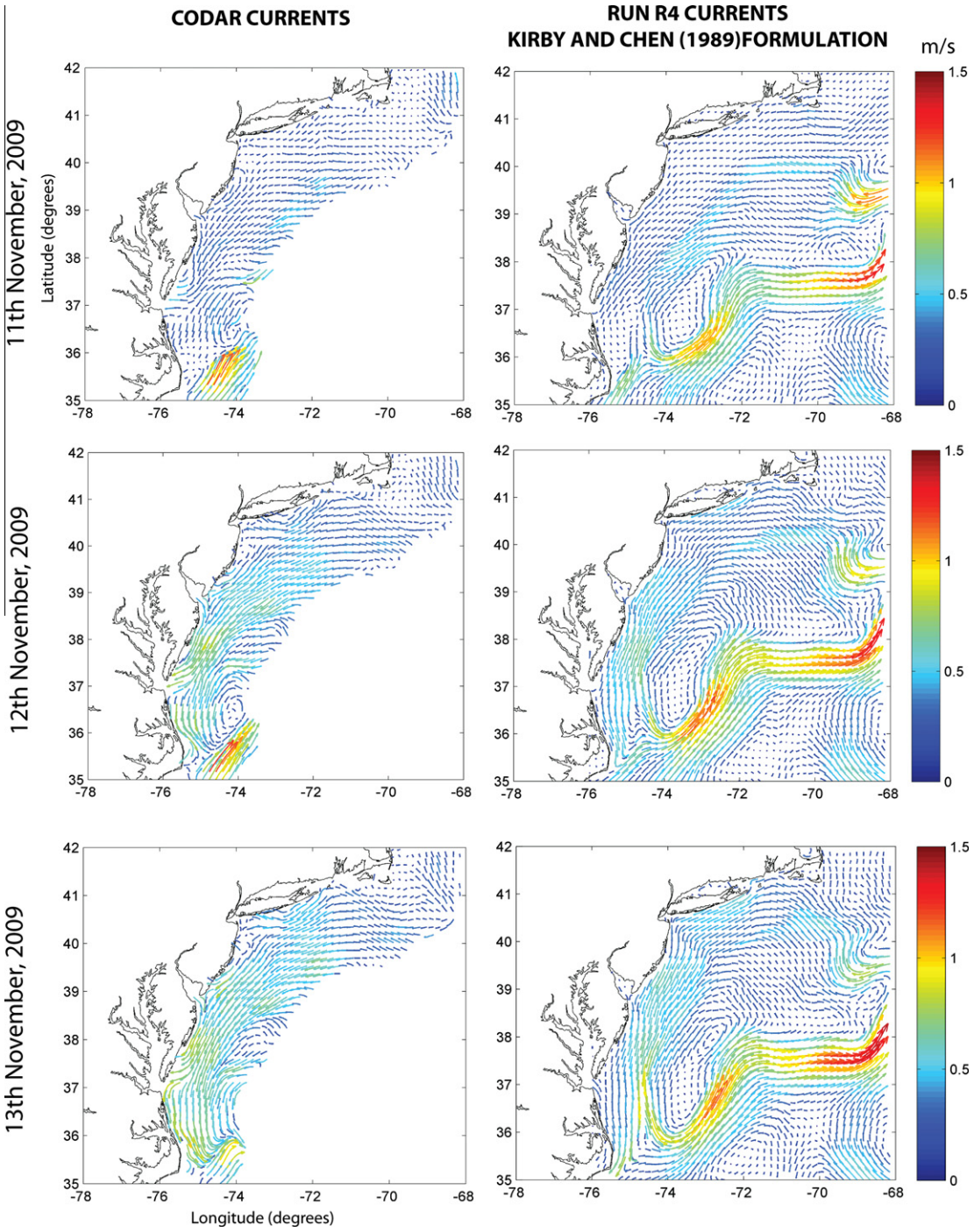

Fig. 18. Daily mean average surface currents in the area between Cape Hatteras and Cape Cod. (a) 11th of November, 2009; (b) 12th of November, 2009; (c) 13th of November, 2009. Left panels represent the CODAR measurements and the right panels represent the daily mean average surface currents computed in run R4 using the Kirby and Chen (1989) formulation.

results could also be identified, especially near the coast. For example, near the mouth of the Oregon Inlet, the model did not correctly capture the intensity and direction of the currents. The numerical resolution in this area was not fine enough to correctly reproduce the water exchange through the inlet. Despite the mentioned discrepancies, in general, a good agreement between the computed and measured surface currents was obtained, particularly when using the TY2001 closure model (Table 4). The RMSE varied between 0.18 and 0.11 m s^{-1} depending on the surface roughness closure model. The model error was higher when the effect of ocean surface roughness was not considered. When including the effect of the ocean waves, the RMSE decreased to approximately 0.11 m·s^{-1} and the skill increased to 0.82. The highest model skill values were obtained for the TY2001 parameterization. However, the values of the skill and the RMSE were similar using DGHQ and TY2001.

It is also worth mentioning that to correctly estimate the currents in the region offshore of the shelf, it was necessary to correctly represent the vertical structure of the currents in the top-most portion of the water column. This required a vertical stretching function for the s coordinate that increased the model surface resolution. In the deepest areas, where the waves are

Table 4
Model skill in the location of the Codar measurements.

	RMSE (m/s)	Skill
R2		0.61
	0.17	0.53
	0.68	0.37
	2.02	0.76
	1.88	0.74
	1.11	0.78
R3	0.12	
	0.41	0.8
	0.54	0.65
	1.3	0.85
	1.35	0.81
	1.22	0.77
R4	0.11	0.82
	0.41	0.74
	0.52	0.72
	1.13	0.88
	1.22	0.83
	1.08	0.8
R5	0.18	0.74
	0.47	0.8
	1.04	0.88
	0.94	0.88
	1	0.81

deep-water waves, the currents that mostly affect the gravity-wave dispersion relationship are the currents in the uppermost part of the water column. If the model resolution near the surface is not good enough, the thickness of the first model's vertical layer can be too thick and the currents might be underestimated.

Scatter plots between the measurements and computed surface currents for the 13th of November (Fig. 19) showed that with the CHNK model (run R2), the surface currents were generally underpredicted. The OOST closure model (run R5) produced the strongest currents with intensities higher than those observed in the measurements. The best agreement with the measurements (as determined by the values of the model skill and RMSE) was obtained with TY2001 (R4).

3.4.3. Storm surge

The storm surge is the sea level response to the combined effect of winds blowing over the ocean and the horizontal and temporal gradients of the atmospheric pressure, which creates an inverse barometer effect. The severity of the storm surge depends on the intensity of the wind forcing, the spatial gradients of the atmospheric pressure, the duration of the storm event, and on the configuration of the coast. Fig. 20 compares the measured and computed storm surge values at each of the characteristic stations (Fig. 2(b)).

The highest storm surge values were observed at the MEX, CHSH and SHCC stations. The surge at MEX reached values of 0.8 m on November 11th. The surge generated during Nor'Ida was higher, up to 1.5 m in the mouth of the Chesapeake Bay. Although a better agreement with the measurements was obtained when the effect of the ocean roughness was included, at most stations, the differences between numerical runs were small. However, at the station with the highest storm surge value (CHSH), neglecting the effect of ocean roughness resulted in the maximum storm surge value being underestimated by 0.4 m. With DGHQ (R3) and TY2001 (R4), the maximum value of the surge was correctly predicted, and with OOST (R5), it was overestimated by 0.5 m. The ocean roughness reduces the value of the wind intensity, but the ocean surface shear stress (forcing the upper ocean column) depends on the roughness. As previously described, the OOST closure model produced the highest reduction in the wind intensity, but it also resulted in the highest surface roughness values and therefore the highest shear stress values and momentum transfer to the ocean currents (Fig. 21).

Table 5 shows the RMSE and the model skill at each characteristic station for each characteristic run. In general, except at the MAINE station, DGHQ (R3) and TY2001 (R4), reduced the root mean square error and increased the model skill considerably.

4. Integrated hydrograph and integrated significant wave height sensitivity

As previously mentioned in the introduction section, a high correlation has been found between the integrated hydrograph and wave height and the storm damage potential. These parameters are defined as the cumulative values of the sea surface elevation and the significant wave height, respectively, during the storm. To analyze the sensitivity of these parameters to the ocean–atmosphere interface fluxes, the period corresponding to Nor'Ida was selected. The integrated hydrograph and wave height were computed for the period between November 12th and 15th for each numerical run. Both parameters are highly sensitive to the interactions between the modules. As an example, Fig. 22 depicts the integrated hydrograph (upper panel) for runs R1 and R5 and the difference between the two runs.

The integrated hydrograph in the coastal area represents the storm surge, while offshore, it represents the sea surface elevation variations associated with macro- and mesoscale oceanic features. In run R1, in which WRF did not consider the effect of the high-resolution SST and ocean roughness, the integrated hydrograph in the area between Cape Hatteras and Cape Cod showed lower values

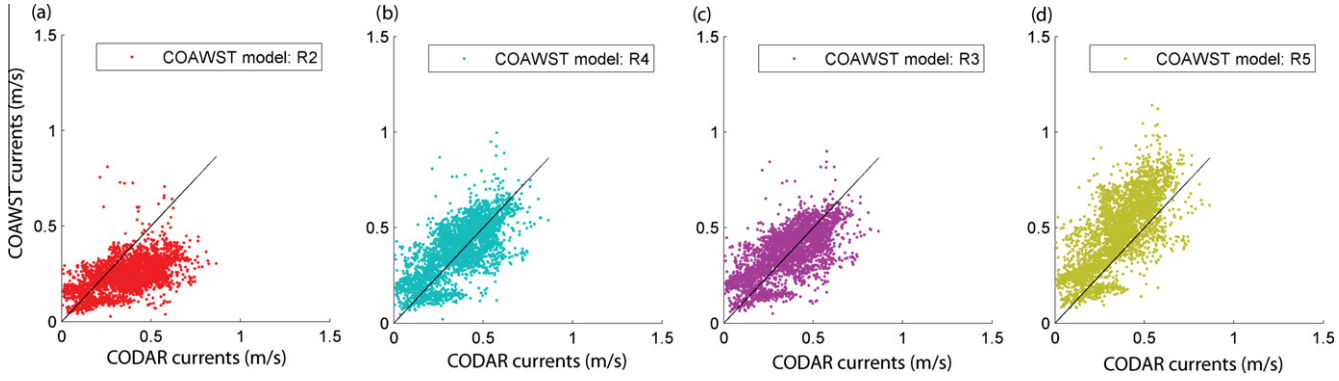

Fig. 19. Scatter plots for the daily average surface currents (13th of November): (a) run R2, in which the high resolution SST data provided by ROMS is included in WRF; (b) run R3, a fully coupled run with the DGHQ closure model; (c) run R4, a fully coupled run with TY2001 closure model; (d) run R5, a fully coupled run with OOST closure model.

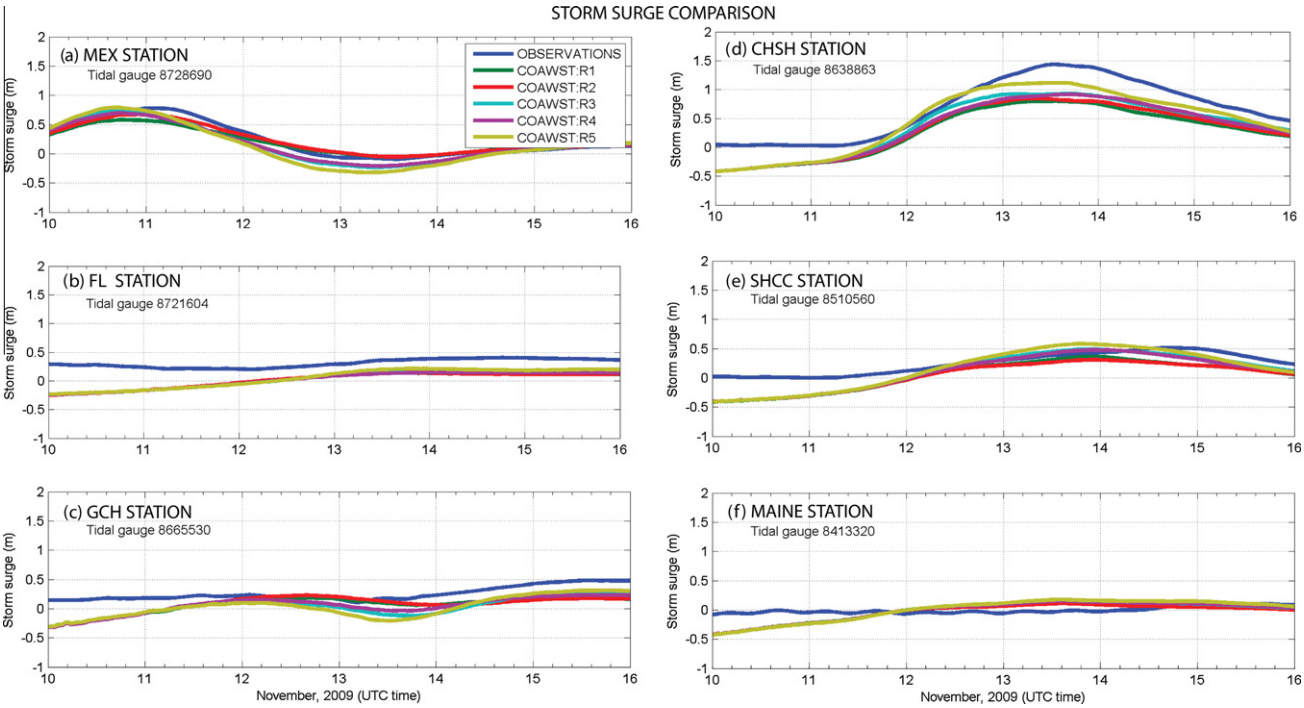

Fig. 20. Comparison of the measured and computed storm surge values time series.

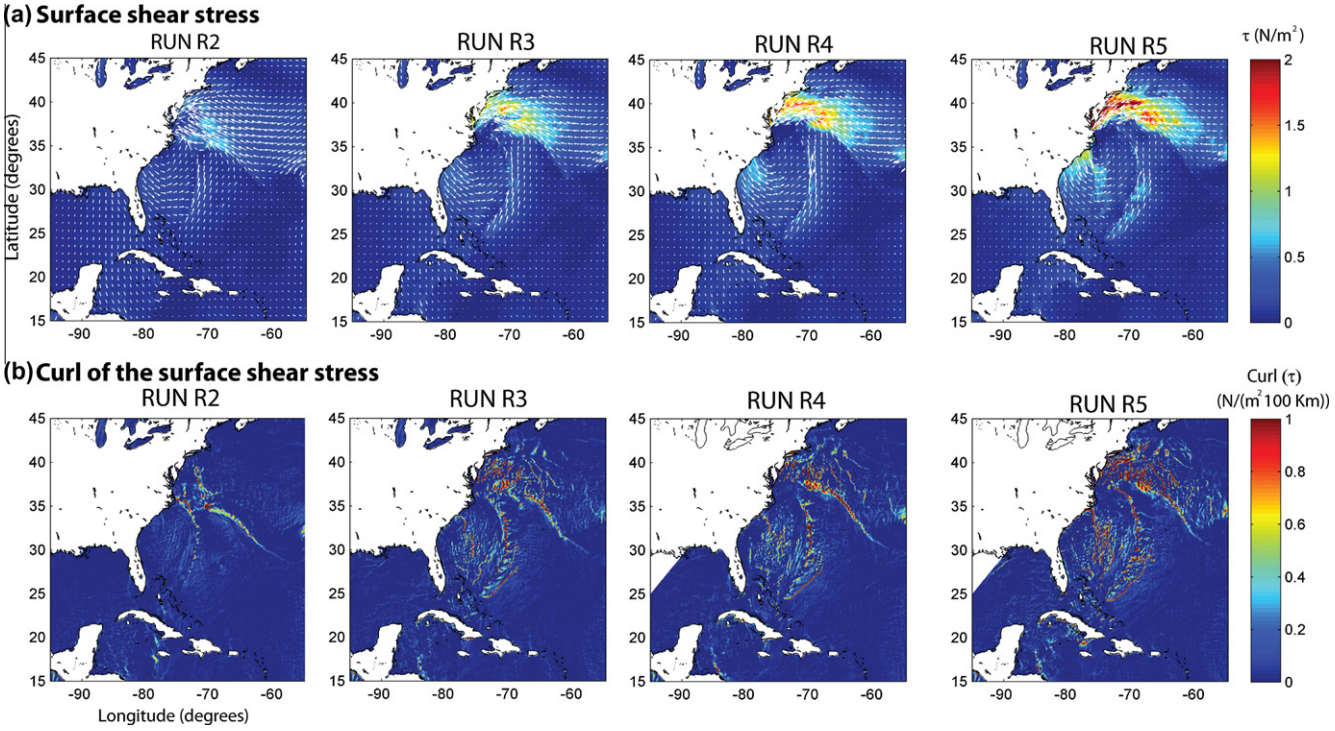

Fig. 21. Spatial distribution of the (a) wind shear stress and (b) wind shear curl for runs R2 (in which the high resolution SST data provided by ROMS is included in WRF), R3 (the fully coupled run with the DGHQ closure model), R4 (the fully coupled run with TY2001 closure model), and R5 (the fully coupled run with OOST closure model).

(up to 1 m·day). The integrated hydrograph can change up to 50% depending on the wave–ocean–atmosphere interactions. The integrated significant wave height (panels in the bottom) also showed a high dependency on such interactions, with changes of up to 40% in the area most affected by the nor'easter.

5. Summary and conclusions

The ocean and atmospheric dynamics during Hurricane Ida and its transition to the Nor'Ida coastal storm were investigated. COAWST, the coupled ocean–wave–atmosphere–sediment transport

Table 5
Model skill in the characteristic stations.

	RMSE (m)						Skill					
	MEX skill	FL skill	GCH skill	CHSH skill	SHCC skill	MAINE skill	MEX RMSE	FL RMSE	GCH RMSE	CHSH RMSE	SHCC RMSE	MAINE RMSE
R1	0.03	0.11	0.11	0.07	0.06	0.38	0.51	0.35	0.62	0.6	0.39	0.06
R2	0.04	0.11	0.08	0.08	0.06	0.32	0.08	0.16	0.26	0.17	0.09	0.06
R3	0.05	0.11	0.07	0.04	0.07	0.37	0.53	0.56	0.86	0.84	0.47	0.05
R4	0.06	0.11	0.05	0.05	0.07	0.35	0.47	0.51	0.9	0.77	0.48	0.06
R5	0.08	0.06	0.22	0.4	0.35	0.42	0.13	0.12	0.35	0.2	0.14	0.04

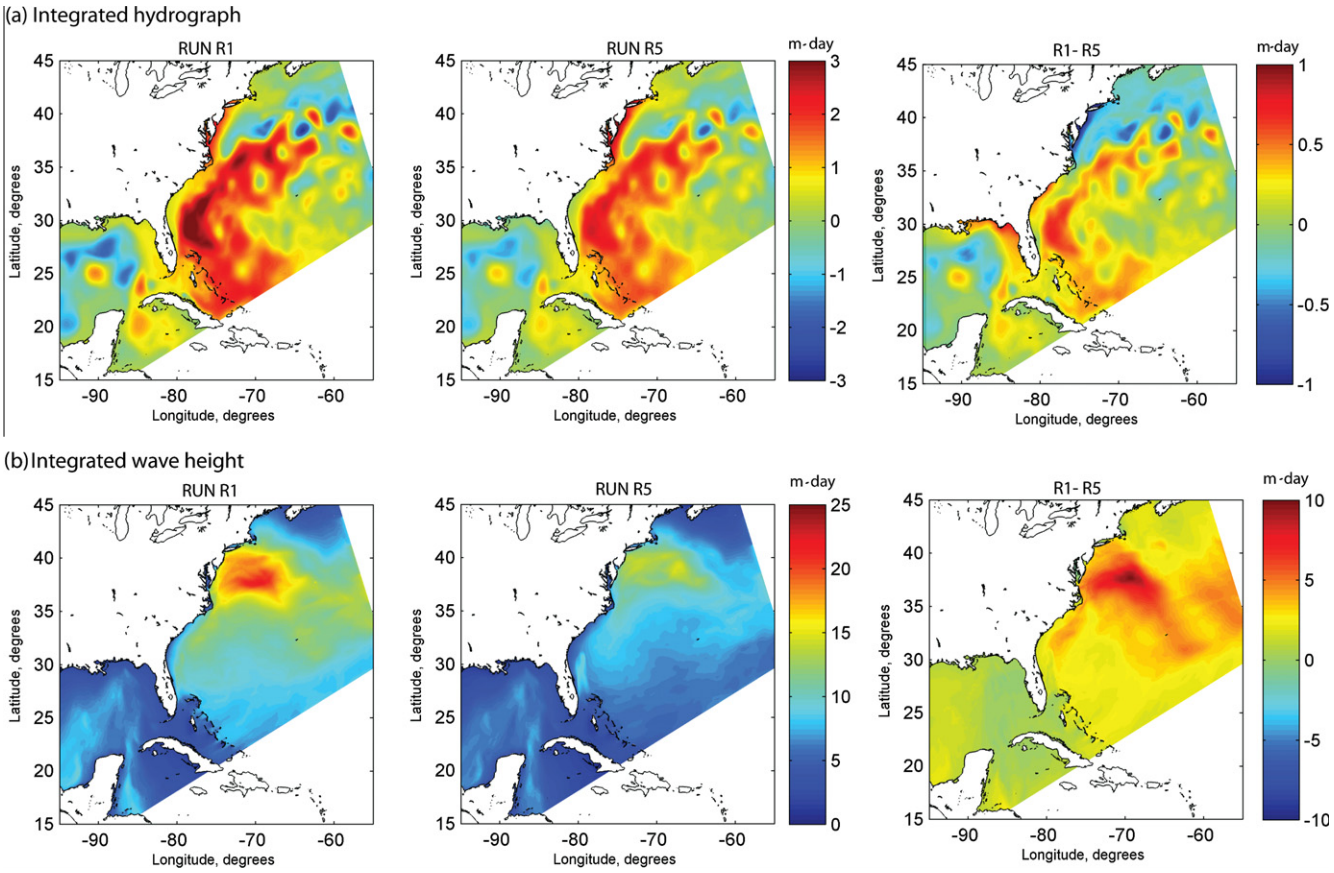

Fig. 22. (a) Integrated hydrograph during Nor'Ida (12–14th of November, 2009). Left panel depicts the results from run R1; middle panel depicts the results from run R5 and right panel shows the difference between R1 and R5. (b) Integrated significant wave height during Nor'Ida (12–14th November, 2009) from the different numerical experiments. Left panel depicts the results from run R1; middle panel depicts the results from run R5 and right panel shows the difference between R1 and R5.

model (Warner et al., 2010), was applied and compared to tide gauge, wave buoy, CODAR, and satellite measurements. Several numerical experiments were run to analyze the role of the interactions between the atmosphere and the ocean.

The fully coupled model correctly captured and reproduced the main atmospheric and ocean dynamics in this combined extreme event. Numerical results captured Ida passing the Yucatan channel, propagating through the Gulf of Mexico and losing energy, and making landfall at 12:00 UTC on the 10th of November. Thereafter, the model was capable of reproducing the movement of this low pressure cell northeastward until it reached the Cape Hatteras region. As in the measurements, the model results indicated that the peak of Nor'Ida occurred on the 13th of November, with wave heights up to 8 m in the most affected area.

Agreement between the model and direct (wind, wave, water level, and current) measurements was improved when the interactions for the ocean module and the wave module were activated in the atmospheric module. The high-resolution SST tended to intensify the winds during Nor'Ida, with a minor effect on Hurricane Ida. Its effect was not as significant as the effect of the wave-induced ocean roughness. Wave roughness generated two opposing effects, described by Zhang and Perrie (2001), on the analyzed storm system. The first effect transferred momentum from the atmosphere to the ocean by reducing the wind intensity in areas with energetic wind waves. This effect had a great impact on the evolution of Ida, reducing the wind field associated with the hurricane as well as its asymmetry. The second effect influenced thermal interactions by enhancing heat and moisture fluxes to the atmosphere.

In the offshore region, hurricane tracks were insensitive to the ocean wave roughness (as identified by Doyle 2002). However, prior to landfall the increased surface roughness caused the cyclone to deviate eastwards, changing the landfall point. This effect could be related to the changes of the precipitation bands due to heat and moisture flux enhancement. However, it could also be related to the hurricane wind asymmetry change. Xiang and Wu (2005) showed that wind asymmetry can affect tropical cyclone

tracks. When the TC is axisymmetric, the storm deflects to the right and the overall trend is east. When the TC is asymmetric but the asymmetry is not sharp, wherever the area of maximum wind is, it deflects to the northwest first and then to various areas depending on the position of the areas of maximum wind. In the case of Ida, wind structure and asymmetry were greatly affected by the wave-induced ocean roughness and this could explain the observed differences. However, this effect needs to be further analyzed.

During the first day of the formation of Nor'Ida, the wind intensity increased due to the effect of the wave-induced roughness in the East Gulf of Mexico and East Florida. This unexpected increase in the wind intensity was related to the change in intensity, location, and extension of the main low pressure system. During the propagation of the remnants of Ida along the coast of Florida and the Gulf of Mexico, the young and steep waves increased the ocean roughness, enhancing the heat and moisture fluxes from the warm waters transported by the Gulf Stream to the atmosphere. Another example of a cyclone that followed the path of the Gulf Stream and intensified in the area between Florida and South Carolina was Hurricane Irene (1999). This enhancement resulted in deepening of the low pressure system, the change of its eye position during Nor'Ida, and the seaward translation of the rain bands associated with the cyclone.

During the analyzed event, two maxima were identified in the wind wave generation processes, one during the passage of Ida through the Gulf of Mexico and one during Nor'Ida. Comparison of wave heights determined by modeling with data from buoys and satellites indicated that the ocean surface roughness reduced the wind speed and consequently, the energy transfer to the waves, resulting in smaller wave heights. The decrease of wind intensities and the consequent wave energy due to the wave-induced ocean surface enhancement is consistent with earlier atmosphere–wave numerical experiments (Webber et al., 1993; Doyle, 1995; Janssen and Viterbo, 1996; Lionello et al., 1998; Desjardins et al. 2000; Zhang and Perrie, 2001; Doyle, 2002; Warner et al., 2010).

The comparison of wind intensities and significant wave heights with the NDBC measurements and altimeter data showed that the fully coupled modeling system, particularly when using the OOST closure model, reduced the RMSE and increased the model skill with respect to the results derived when the atmospheric module was not affected by the ocean and wave modules. The spatial and temporal patterns of the ocean surface roughness estimates by the different closure models were similar, but the OOST spatial gradients were more pronounced and the roughness values were higher than those obtained with DGHQ and TY2001. These more intense gradients and higher roughness values provided a better estimation of the wind intensities. Because OOST considers the effect of wave steepness and wave age, it represents a roughness field that merges those variations observed in DGHQ (which only considers the effect of the wave age) and those in TY2001 (which depends on wave steepness).

The SST comparison with the GOES images showed that the coupled modeling system provides a reasonable estimation of the SST. Both the satellite images and the numerical results showed that Nor'Ida generated eastward displacement of the Gulf Stream in the area of Cape Hatteras, and the Gulf Stream became more meandering.

Daily mean averaged CODAR data were used to analyze the surface currents between Cape Hatteras and Cape Cod during Nor'Ida. COAWST agrees with the observations, showing that during the storm, the currents over much of the mid-Atlantic shelf region were directed southwestward and veered southeastwards offshore from North Carolina. In general, the numerical results agreed well with the CODAR measurements, although some local differences could also be identified (e.g., close to the Oregon inlet mouth). The fully coupled results captured the Gulf Stream displacement due to currents formed during the storm in the shelf region. The numerical runs demonstrated that the surface currents can change up to 0.3 m s^{-1} depending on the closure model for the ocean surface roughness used (using the OOST closure model, the surface currents were over predicted).

The modeled storm surge value was in agreement with the measurements, especially in the coupled runs. During the analysis period, the maximum storm surge occurred in the region between Cape Hatteras and Virginia with values of up to 1.5 m. In this region, TY2001 and DGHQ provided the best estimates of the surge maxima. The integrated hydrograph computed for the Nor'Ida event also showed a clear storm surge in this region. The horizontal extent of the storm surge varied depending on the interactions considered in the numerical runs, producing differences of up to 50% of the computed values. The same trend was observed in the integrated significant wave height.

This research demonstrates the capability of the COAWST modeling system to simulate the air–sea-wave dynamics during extreme events such as hurricanes and nor'easter storms without including data assimilation. It has also shown how important the interactions between the ocean waves and the atmospheric boundary layer are, not only for the prediction of the wind intensity, but also for capturing the ocean state.

This study has revealed that although the inclusion of ocean roughness in the atmospheric module improves the prediction of winds, the waves and the storm surge, the closure model providing the best results for the winds and waves does not necessarily coincide with the parameterization that provide the best results for the surface currents and storm surge values. In the current version of COAWST, both WRF and ROMS use the same parameterization of the ocean surface shear stress. However, SWAN directly uses the wind fields and computes the stresses according to Wu (1982). The results derived in this study suggest the need for using the same parameterization in all the modules.

Acknowledgements

Primary funding for this study was furnished by the US Geological Survey, Coastal and Marine Geology Program, under the Carolinas Coastal Processes Project. We are also grateful to the Career Training Interexchange program that facilitated the training period of Maitane Olabarrieta within the USGS. The tidal gauge data used were derived from the National Tidal Gauge database and the wave and wind information were obtained from the National Buoy Database. Both databases are operated by the NOAA. Surface wind analysis data were obtained from the Hurricane Research Division of NOAA. Altimeter products were produced by Ssalto/Duacs and distributed by Aviso, with support from Cnes. CODAR products were produced and distributed within the MARCOOS project. The SST data used in the present analysis were distributed by the NOAA CoastWatch project. We would also like to thank the developers of T_Tide, WAFO toolbox and of the SWAN, WRF, and ROMS models. We are grateful to the three anonymous reviewers for their helpful suggestions.

Appendix A

The three parameterizations used for the ocean surface roughness considered in the paper are briefly described.

A.1. Taylor and Yelland (2001, TY2001)

Taylor and Yelland (2001) proposed a wave steepness-based parameterization for the ocean roughness based on three datasets

representing sea-state conditions ranging from strongly forced to shoaling. The parameterization is given by the following equation:

$$\frac{z_0}{H_s} = 1200(H_s/L_p)^{4.5} \quad (1.1)$$

where L_p represents the wavelength at the peak of the wave spectrum, H_s the significant wave height and z_0 the ocean roughness.

The formula has been found to well describe a variety of datasets, both field and laboratory, with the notable exception of short fetch (Drennan et al., 2005).

A.2. Drennan et al. (2003, DGHQ)

Drennan et al. (2003) proposed a wave age-based formula to characterize the ocean roughness. To derive this formula, the authors combined data from many field experiments representing a variety of conditions and grouped the data as a function of the wind friction velocity (u_*). Their resultant expression is given by

$$\frac{z_0}{H_s} = 3.35(u_*/C_p)^{3.4} \quad (1.2)$$

where *Cp* is the wave phase speed at the peak frequency. This equation was found to fit their pure wind-sea, rough-flow, deep-water dataset quite well (Drennan et al., 2005).

A.3. Oost et al. (2002)

Based on the 1996 ASGAMAGE experiment, Oost et al. (2002) derived the following expression for the ocean roughness:

$$\frac{z_0}{L_p} = \frac{25.0}{\pi}(u_*/C_p)^{4.5} \quad (1.3)$$

Although this expression is dependent on the wave age, it also considers the effect of the wave steepness.

References

Aldrian, E., Sein, D.V., Jacob, D., Gates, L.D., Podzun, R., 2005. Modeling Indonesian rainfall with a coupled regional model. Climate Dyn. 25, 1–17.

Avila, L.A., Cangialosi, J., 2010. Tropical Cyclone Report. Hurricane Ida (AL112009), 14 January 2010. National Hurricane Center.

Bender, M.A., Ginis, I., 2000. Real-case simulations of hurricane–ocean interaction using a high-resolution coupled model: effects on hurricane intensity. Mon. Weather Rev. 128, 917–946.

Bender, M.A., Ginis, I., Tuleya, R., Thomas, B., Marchok, T., 2007. The operational GFDL coupled hurricane–ocean prediction system and a summary of its performance. Mon. Weather Rev. 135, 3965–3989.

Booij, N., Ris, R.C., Holthuijsen, L.H., 1999. A third-generation wave model for coastal regions, part I. Model description and validation. J. Geophys. Res. 104 (C4), 7649–7666.

Cavaleri, L., Sclavo, M., 2006. The calibration of wind and wave model data in the Mediterranean Sea. Coast. Eng. 53, 613–627.

Charnock, H., 1955. Wind stress on a water surface. Q. J. R. Meteorol. Soc. 81, 639.

Chassignet, E.P., Arango, H.G., Dietrich, D., Ezer, T., Ghil, M., Haidvogel, D.B., Ma, C.-C., Mehra, A., Paiva, A.M., Sirkes, Z., 2000. DAMEE-NAB: the base experiments. Dyn. Atmos. Oceans 32, 155–183.

Chen, S.S., Price, J.F., Zhao, W., Donelan, M.A., Walsh, E.J., 2007. The CBLAST-hurricane program and the next-generation fully coupled atmosphere–wave–ocean models for hurricane research and predictions. Bull. Am. Meteorol. Soc. 88, 311–317.

Chen, Q., Wang, L., Zhao, H., 2008. An integrated surge and wave modeling system for Northern Gulf of Mexico: simulations for Hurricanes Katrina and Ivan. In: Proceedings of the International Conference on Coastal Engineering. ASCE, pp. 1072–1084.

Desjardins, S., Mailhot, J., Lalbeharry, R., 2000. Examination of the impact of a couple atmospheric and ocean wave system, part I. Atmospheric aspects. J. Phys. Oceanogr. 30, 385–401.

Dolan, R., Davis, R.E., 1994. Coastal storm hazards. In: Finkl, C. (Ed.), Coastal Hazards Perception, Susceptibility, and Mitigation. J. Coast. Res. 12 (Special issue), 103–114.

Dolan, R., Hayden, B., 1981. Storms and shoreline configuration. J. Sediment. Petrol. 51, 737–744.

Donelan, M.A., Dobson, F.W., Smith, S.D., Anderson, R.J., 1993. On the dependence of sea-surface roughness on wave development. J. Phys. Oceanogr. 23, 2143–2149.

Döscher, R., Willén, U., Jones, C., Rutgersson, A., Meier, H.E.M., Hansson, U., Graham, L.P., 2002. The development of the regional coupled ocean–atmosphere model RCAO. Boreal Environ. Res. 7, 183–192.

Doyle, J.D., 1995. Coupled ocean wave/atmosphere mesoscale model simulations of cyclogenesis. Tellus 47A, 766–788.

Doyle, J.D., 2002. Coupled atmosphere–ocean wave simulations under high wind conditions. Mon. Weather Rev. 130, 3087–3099.

Drennan, W.M., Graber, H.C., Hauser, D., Quentin, C., 2003. On the wave age dependence of wind stress over pure wind seas. J. Geophys. Res. 108, 8062. doi:10.1029/2000JC000715.

Drennan, W.M., Taylor, P.K., Yelland, M.J., 2005. Parameterizing the sea surface roughness. J. Phys. Oceanogr. 35, 835–848.

Fan, Y., Ginis, I., Hara, T., Wright, C.W., Walsh, E.J., 2009b. Numerical simulations and observations of surface wave fields under extreme tropical cyclone. J. Phys. Oceanogr. 39, 2097–2116.

Feddersen, F., Trowbridge, J.H., 2005. The effect of breaking on surf-zone turbulence and alongshore currents: a modeling study. J. Phys. Oceanogr. 35, 2187–2203.

Flather, R.A., 1976. A tidal model of the north-west European continental shelf. Memoires de la Societe Royale des Sciences de Liege 6 (10), 141–164.

Funakoshi, Y., Hagen, S.C., Bacopoulos, P., 2008. Coupling of hydrodynamic and wave models: a case study for a Hurricane Floyd (1999) Hindcast. J. Waterw. Port Coast. Ocean Eng. 134 (6 2008 32). doi:10.1061/(ASCE)0733-950X.

Gemmill, W., Katz, B., Li, X., 2007. Daily Real-Time Global Sea Surface Temperature–High Resolution Analysis at NOAA/NCEP. NOAA/NWS/NCEP/MMAB Office Note Number 260, p. 39.

Gong, D., Kohut, J.T., Glenn, S.M., 2010. Seasonal climatology of wind driven circulation on the New Jersey Shelf. J. Geophys. Res. 115, C04006.

Gourrion, J., Vandemark, D., Bailey, S., Chapron, B., Gommenginger, G.P., Challenor, P.G., Srokosz, M.A., 2002. A two-parameter wind speed algorithm for ku-band altimeters. J. Atmos. Ocean. Technol. 19, 2030–2048.

Grosskopf, W.G., Bass, G.P., 2010. The great Mid-Atlantic Storm of 2009: 'Friday the 13th' storm impacts on Ocean City, Maryland. Shore Beach. 78 (2), 12–19.

Gustafsson, N., Nyberg, L., Omstedt, A., 1998. Coupling of a high-resolution atmospheric model and an ocean model for the Baltic Sea. Mon. Weather Rev. 126, 2822–2846.

Hagedorn, R., Lehmann, A., Jacob, D., 2000. A coupled high resolution atmosphere–ocean model for the BALTEX region. Meteorol. Z. 9, 7–20.

Haidvogel, D.B., Arango, H.G., Hedstrom, K., Beckmann, A., Malanotte-Rizzoli, P., Shchepetkin, A.F., 2000. Model evaluation experiments in the North Atlantic Basin: Simulations in nonlinear terrain-following coordinates. Dyn. Atmos. Oceans 32, 239–281.

Haidvogel, D.B., Arango, H.G., Budgell, W.P., Cornuelle, B.D., Curchitser, E., Di Lorenzo, E., Fennel, K., Geyer, W.R., Hermann, A.J., Lanerolle, L., Levin, J., McWilliams, J.C., Miller, A.J., Moore, A.M., Powell, T.M., Shchepetkin, A.F., Sherwood, C.R., Signell, R.P., Warner, J.C., Wilkin, J., 2008. Regional ocean forecasting in terrain-following coordinates: model formulation and skill assessment. J. Comput. Phys.

Hara, T., Belcher, S.E., 2002. Wind forcing in the equilibrium range of wind-wave spectra. J. Fluid Mech. 470, 223–245.

Herrington, T.O., Miller, J.K., 2010. A comparison of methods used to calculate northeaster damage potential. Shore Beach. 78 (2), 20–25.

Intergovernmental Panel of Climate Change (IPCC), 2007. Climate change 2007: the physical science basis. In: Solomon, S., Qin, D., Manning, M., Chen, Z., Marquis, M., Averyt, K.B., Tignor, M., Miller, H.L. (Eds.), Contribution of Working Group I to the Fourth Assessment Report of the Intergovernmental Panel on Climate Change. Cambridge University Press, Cambridge, United Kingdom, New York, NY, USA.

Irish, J.L., Resio, D.T., 2010. A hydrodynamics-based surge scale for hurricanes. Ocean Eng. 37, 69–81.

Jacob, R., Larson, J., Ong, E., 2005. M × N Communication and parallel interpolation in community climate system model version 3 using the model coupling toolkit. Int. J. High Perform. Comput. Appl. 19 (8), 293–307.

Janssen, P.A.E.M., 1989. Wave induced stress and the drag of air flowover sea waves. J. Phys. Oceanogr. 19, 745–754.

Janssen, P.A.E.M., Viterbo, P., 1996. Ocean waves and the atmospheric climate. J. Climate 9, 1269–1287.

Jones, P.W., 1998. A User Guide for Scrip: A Spherical Coordinate Remapping and Interpolation Package, Version 1.4. Los Alamos National Laboratory. <http://climate.lanl.gov/Software/SCRP/>.

Kain, J.S., Fritsch, J.M., 1993. Convective parameterization for mesoscale models: the Kain–Fritsch scheme. The representation of cumulus convection in numerical models. Meteor. Monogr. 24, 165–170.

Kim, S.Y., Yasuda, T., Mase, H., 2010. Wave set-up in the storm surge along open coasts during Typhoon Anita. Coast. Eng. 57 (7), 631–642.

Kirby, J.T., Chen, T.-M., 1989. Surface waves on vertically sheared flows: approximate dispersion relations. J. Geophys. Res. 94, 1013–1027.

Komen, G.J., Hasselmann, S., Hasselmann, K., 1984. On the existence of a fully developed wind-sea spectrum. J. Phys. Oceanogr. 14, 1271–1285.

Kumar, N., Voulgaris, G., Warner, J.C., Olabarrieta, M., 2012. Implementation of the vortex force formalism in the Coupled Ocean-Atmosphere-Wave-Sediment Transport (COAWST) modeling system for inner shelf and surf zone applications. Ocean Modell. in press. doi:10.1016/j.ocemod.2012.01.003.

Larson, J., Jacob, R., Ong, E., 2004. The Model Coupling Toolkit: a new Fortran90 Toolkit for building multiphysics parallel coupled models. Int. J. High Perform. Comput. Appl. 19 (8), 277–292.

Lee, G.H., Nicholls, R.J., Birkemeier, W.A., 1998. Storm-driven variability of the beach–nearshore profile at Duck, North Carolina, USA, 1981–1991. Mar. Geol. 148 (3–4), 163–177.
Lin, Y.-L., Farley, R.D., Orville, H.D., 1983. Bulk parameterization of the snow field in a cloud model. J. Climate Appl. Meteorol. 22, 1065–1092.
Lionello, P., Malguzzi, P., Buzzi, A., 1998. Coupling between the atmospheric circulation and ocean wave field: an idealized case. J. Phys. Oceanogr. 28, 161–177.
Liu, W.T., Katsaros, K.B., Businger, J.A., 1979. Bulk parameterization of the air–sea exchange of heat and water vapor including the molecular constrains al the interface. J. Atmos. Sci. 36, 1722–1735.
Loglisci, N., Qian, M.W., Rachev, N., Cassardo, C., Longhetto, A., Purini, R., Trivero, P., Ferrarese, S., Giraud, C., 2004. Development of an atmosphere–ocean coupled model and its application over the Adriatic Sea during a severe weather event of Bora wind. J. Geophys. Res. 109, D01102. doi:10.1029/2003JD003956.
Madsen, O.S., 1994. Spectral wave-current bottom boundary layer flows: coastal engineering 1994. In: Proceedings of the 24th International Conference. Coastal Engineering Research Council/ASCE, pp. 384–398.
Marks, F., Shay, L.K., 1998. Landfalling tropical cyclones: forecast problems and associated research opportunities: report of the 5th Prospectus Development Team to the US Weather Research Program. BAMS 79, 305–323.
Mastenbroek, C., Burgers, G., Janssen, P.A.E.M., 1993. The dynamical coupling of a wave model and a storm surge model through the atmospheric boundary layer. J. Phys. Oceanogr. 23, 1856–1866.
Mikolajewicz, U., Sein, D.V., Jacob, D., Konigk, T., Pozdun, R., Semmler, T., 2005. Simulating Arctic sea ice variability with a coupled regional atmosphere–ocean–sea ice model. Meteorol. Z. 14, 793–800.
Munger, S., Kraus, N.C., 2010. Frequency of extreme storms based on beach erosion at Northern Assateague Island, Maryland. Shore Beach 78 (2), 3–11.
Nakanishi, M., Niino, H., 2004. An improved Mellor–Yamada level-3 model with condensation physics: its design and verification. Bound. Lay. Meteorol. 112, 1–31.
Nakanishi, M., Niino, H., 2006. An improved Mellor–Yamada level-3 model: its numerical stability and application to a regional prediction of advection fog. Bound. Lay. Meteorol. 119, 397–407.
Nakanishi, M., Niino, H., 2009. Development of an improved turbulence closure model for the atmospheric boundary layer. J. Meteorol. Soc. Jpn. 87, 895–912.
Nakanishi, M., 2001. Improvement of Mellor–Yamada turbulence closure model based on large-eddy simulation data. Bound. Lay. Meteorol 99, 349–378.
Oost, W.A., Komen, G.J., Jacobs, C.M.J., van Oort, C., 2002. New evidence for a relation between wind stress and wave age from measurements during ASGAMAGE. Bound. Lay. Meteorol. 103, 409–438.
OSTM/Jason-2 Products Handbook, 2009. <http://www.eumetsat.int/Home/Main/Satellites/Jason-2/Resources/index.htm>, EUM.OPS-JAS.MAN.08.0041.
Perrie, W., Zhang, Y., 2001. A regional climate model coupled to ocean waves: synoptic to multi-monthly simulations. J. Geophys. Res. 106 (D16), 17753–17771.
Perrie, W., Ren, X., Zhang, W., Long, Z., 2004. Simulation of extratropical Hurricane Gustav using a coupled atmosphere–ocean-sea spray model. Geophys. Res. Lett. 31, L03110, 1029/2003GL018571.
Perrie, W., Andreas, E.L., Zhang, W., Li, W., Gyakum, J., McTaggart-Cowan, R., 2005. Impact of sea spray on rapidly intensifying cyclones at midlatitudes. J. Atmos. Sci. 62, 1867–1883.
Powell, M.D., Houston, S.H., 1996. Hurricane Andrew's landfall in South Florida. Part II: surface wind fields and potential real-time applications. Weather. Forecast. 11, 329–349.
Powell, M.D., Houston, S.H., Reinhold, T.A., 1996. Hurricane Andrew's Landfall in South Florida. Part I: standardizing measurements for documentation of surface wind fields. Weather Forecast. 11, 304–328.
Powers, J.G., Stoelinga, M.T., 2000. A coupled air–sea mesoscale model: Experiments in atmospheric sensitivity to marine roughness. Mon. Weather Rev. 128, 208–228.
Ren, X., Perrie, W., Long, Z., Gyakum, J., McTaggart-Cowan, R., 2004. On the atmosphere–ocean coupled dynamics of cyclones in midlatitudes. Mon. Weather Rev. 132, 2432–2451.
Sallenger, A.H., 2000. Storm impact scale for barrier islands. J. Coast. Res. 16 (3), 890–895.
Schrum, C., Hübner, U., Jacob, D., Podzun, R., 2003. A coupled atmosphere/ice/ocean model for the North Sea and Baltic Sea. Climate Dyn. 21, 131–141.
Seo, H., Miller, A.J., Roads, J.O., 2007. The scripps coupled Ocean–Atmosphere regional (SCOAR) model, with applications in the eastern Pacific sector. J. Climate 20, 381–402.
Shchepetkin, A.F., McWilliams, J.C., 2005. The Regional Ocean Modeling System (ROMS): a split-explicit, free-surface, topography-following-coordinates ocean model. Ocean Modell. 9, 347–404.
Sheng, Y.P., Alymov, V., Paramygin, V.A., 2010. Simulation of storm surge, wave, currents, and inundation in the Outer Banks and Chesapeake Bay during Hurricane Isabel in 2003: the importance of waves. J. Geophys. Res. 115, C04008. doi:10.1029/2009JC005402.
Skamarock, W.C., Klemp, J.B., Dudhia, J., Gill, D.O., Barker, D.M., Wang, W., Powers, J.G., 2005. A Description of the Advanced Research WRF, Version 2, NCAR Technical Note, NCAR/TN-468+STR.
Smith, S.D., 1988. Coefficients for the sea surface stress, heat flux, and wind profiles as a function of wind speed and temperature. J. Geophys. Res. 993, 15467–15472.
Stacey, M.W., 1999. Simulation of the wind-forced near-surface circulation in knight inlet: a parameterization of the roughness length. J. Phys. Oceanogr. 29, 1363–1367.
Stewart, R.H., Joy, J.W., 1974. HF radio measurement of surface currents. Deep-Sea Res. 21, 1039–1049.
Taylor, P.K., Yelland, M.J., 2001. The dependence of sea surface roughness on the height and steepness of the waves. J. Phys. Oceanogr. 31, 572–590.
Uchiyama, Y., McWilliams, J.C., Shchepetkin, A.F., 2010. Wave-current interaction in an oceanic circulation model with a vortex force formalism: application to the surf zone. Ocean Modell. 34 (1–2), 16–35.
Warner, J.C., Sherwood, C.R., Arango, H.G., Signell, R.P., 2005. Performance of four turbulence closure models implemented using a generic length scale method. Ocean Modell. 8, 81–113.
Warner, J.C., Sherwood, C.R., Signell, R.P., Harris, C.K., Arango, H.G., 2008. Development of a three-dimensional, regional, coupled wave, current, and sediment-transport model. Comput. Geosci. 34 (10), 1284–1306.
Warner, J.C., Armstrong, B., He, R., Zambon, J., 2010. Development of a coupled ocean–atmosphere–wave–sediment transport (COAWST) modeling system. Ocean Modell. 35, 230–244.
Webber, S.L., von Storch, H., Viterbo, P., Zambresky, L., 1993. Coupling an ocean wave model to an atmospheric general circulation model. Climate Dyn. 9, 53–61.
Wilmott, C.J., 1981. On validation of models. Phys. Geogr. 2, 184–194.
Wu, J., 1982. Wind-stress coefficients over sea surface from breeze to hurricane. J. Geophys. Res. 87 (C12), 9704–9706.
Xiang, J., Wu, R., 2005. The effect of asymmetric wind structures of tropical cyclones on their tracks. Acta Meteorologica Sin. 19, 52–59.
Xie, L., Liu, H., Peng, M., 2008. The effect of wave–current interactions on the storm surge and inundation in Charleston Harbor during Hurricane Hugo 1989. Ocean Modell. 20, 252–269.
Yao, Y., Perrie, W., Zhang, W., Jiang, J., 2008. The characteristics of atmosphere–ocean interactions along North Atlantic extratropical storms tracks. J. Geophys. Res. 113, D14124. doi:10.1029/2007JD008854.
Zhang, M.Y., Li, Y.S., 1997. The dynamic coupling of a third-generation wave model and a 3D hydrodynamic model through boundary-layers. Cont. Shelf Res. 17, 1141–1170.
Zhang, Y., Perrie, W., 2001. Feedback mechanism for the atmosphere and ocean surface. Bound. Lay. Meteorol. 100 (2), 321–348.